Submitted to the Astrophysical Journal

Anisotropic Locations of Satellite Galaxies: Clues to the Orientations of Galaxies within their Dark Matter Halos

Ingolfur Agustsson & Tereasa G. Brainerd

Boston University, Institute for Astrophysical Research, 725 Commonwealth Ave., Boston, MA 02215

ingolfur@bu.edu, brainerd@bu.edu

ABSTRACT

We investigate the locations of the satellites of relatively isolated host galaxies in the Sloan Digital Sky Survey and the Millennium Run simulation. Provided we use two distinct prescriptions to embed luminous galaxies within the simulated dark matter halos (ellipticals share the shapes of their halos, while disks have angular momenta that are aligned with the net angular momenta of their halos), we find a fair agreement between observation and theory. Averaged over scales $r_p \leq 500$ kpc, the satellites of red, high–mass hosts with low star formation rates are found preferentially near the major axes of their hosts. In contrast, the satellites of blue, low–mass hosts with low star formation rates show little to no anisotropy when averaged over the same scale. The difference between the locations of the satellites of red and blue hosts cannot be explained by the effects of interlopers in the data. Instead, it is caused primarily by marked differences in the dependence of the mean satellite location, $\langle\phi\rangle$, on the projected distance at which the satellites are found. We also find that the locations of red, high–mass satellites with low star formation rates show considerably more anisotropy than do the locations of blue, low–mass satellites with high star formation rates. There are two contributors to this result. First, the blue satellites have only recently arrived within their hosts' halos, while the red satellites arrived in the far distant past. Second, the sample of blue satellites is heavily contaminated by interlopers, which suppresses the measured anisotropy compared to the intrinsic anisotropy.

Subject headings: dark matter — galaxies: dwarf — galaxies: fundamental parameters — galaxies: halos — galaxies: structure

1. Introduction

The locations of satellite galaxies, measured with respect to the symmetry axes of their hosts, may hold important clues to the formation of large galaxies. This is especially true for Cold Dark Matter (CDM) models in which the dark matter halos of galaxies are mildly flattened, and galaxy formation and mass accretion occur within filaments. Some early studies of the locations of satellite galaxies suggested that satellites had a preference for being located near the minor axes of their hosts (e.g., Holmberg 1969; Zaritsky et al. 1997), an observation that is sometimes known as the "Holmberg effect". Valtonen et al. (1978) found exactly the opposite effect, and concluded that compact satellites tended to be aligned with the major axes of their hosts. Other early studies suggested that any tendency for satellite galaxies to be found in preferred locations was at best rather weak, and perhaps non–existent (e.g., Hawley & Peebles 1975; Sharp et al. 1979; MacGillivray et al. 1982). All of these early studies were based on relatively small samples of between ~ 10 and ~ 200 satellite galaxies and as modern, extensive redshift surveys have become available, the observed number of host–satellite systems has increased enormously. Based upon these large surveys it now appears that, when averaged over all host–satellite pairs, the satellites of relatively isolated host galaxies have a tendency to be found near the major axes of their hosts (see, e.g., Brainerd 2005). There is, however, increasing evidence that the locations of the satellites depend upon host type (e.g., red vs. blue), as well as satellite type.

In an analysis of the locations of the satellites of relatively isolated host galaxies in the Two Degree Field Galaxy Redshift Survey (2dFGRS; Colless et al. 2001, 2003), Sales & Lambas (2004) found a tendency for the satellites of early–type hosts to be located near the major axes of the hosts, while the satellites of late–type hosts were consistent with being distributed isotropically (see the erratum by Sales & Lambas 2009). In addition, they found a tendency for the locations of satellites with low star formation rates to show a greater degree of anisotropy than satellites with high star formation rates. Azzaro et al. (2007, hereafter APPZ) concluded that, as a whole, the satellites of relatively isolated host galaxies in the Sloan Digital Sky Survey (SDSS; Fukugita et al. 1996; Hogg et al. 2001; Smith et al. 2002; Strauss et al. 2002; York et al. 2000) were found preferentially near the major axes of their hosts. Further, APPZ found that the degree of anisotropy was greatest for the red satellites of red host galaxies, while the locations of the satellites of blue host galaxies were consistent with an isotropic distribution. Similar results were found by Siverd et al. (2009) in a more recent analysis of the SDSS, where they showed that the satellites of red, centrally–concentrated hosts are found preferentially close to the major axes of the hosts, and the effect is strongest for red, centrally–concentrated satellites. In a study of extremely isolated SDSS host galaxies, Bailin et al. (2008) found that the satellites of spheroidal host galaxies were located preferentially close to the major axes of the hosts, while the satellites

of blue disk hosts were distributed isotropically.

The dependence of satellite location on the color of the host has also been observed within group environments by Yang et al. (2006, hereafter Yang06), who found that the satellites of red central galaxies in the SDSS had a strong tendency to be aligned with the major axes of the central galaxies, while the satellites of blue central galaxies were distributed isotropically about the central galaxies. Further, Yang06 found that the red satellites of red central galaxies were distributed much more anisotropically than were the blue satellites of red central galaxies, and the degree of anisotropy in the satellite locations increased only weakly with the mass of the surrounding halo.

Here we further investigate the anisotropic distribution of satellite galaxies around relatively isolated hosts, focussing on the dependence of the anisotropy on various physical parameters of the hosts and the satellites (e.g., rest–frame color, specific star formation rate and stellar mass). We also investigate the effects of "interlopers" (i.e., false satellites) on the locations of the satellites, as well as the dependence of satellite location on projected distance from the host. The locations of satellites in the observed Universe are computed using SDSS galaxies, and these are compared to the locations of satellites in the ΛCDM Millennium Run simulation. Our work here is similar in spirit to that of Kang et al. (2007; hereafter Kang07), who used a simulation that combined N-body calculations with semi-analytic galaxy formation to compare the locations of satellite galaxies in a ΛCDM universe to the results obtained by Yang06 for SDSS satellites. Our work differs from that of Kang07 in a number of ways, however. First, we focus on the satellites of relatively isolated host galaxies whereas Yang06 and Kang07 focus primarily on group systems. Second, in our work we use the stellar masses of the host and satellite galaxies when exploring the dependence of the satellite locations on mass. In contrast, Yang06 and Kang07 use a group luminosity function to assign masses to the dark matter halos that surround their groups. Third, we divide our theoretical galaxies into two broad classes, elliptical and non–elliptical, and we use different prescriptions to assign shape parameters to the luminous portions of these galaxies. Kang07, however, did not divide their theoretical galaxies into different classes and they used identical prescriptions to assign shape parameters to the luminous portions of all of their galaxies.

We note that Sales et al. (2007) have also investigated the locations of satellite galaxies of relatively isolated host galaxies in the Millennium Run. Their approach, however, was rather different than our own. Sales et al. (2007) use the full information of the simulation (in particular, 3D distances) to select their hosts and satellites, while we focus on samples that are selected using the same selection criteria that are used to select hosts and satellites from large redshift surveys. Having full 3D information, Sales et al. (2007) selected all satellites

with $M_r < -17$ that were found within the virial radii of their hosts and computed the locations of the satellites. The result was preference for the satellites to populate a plane that is perpendicular to the angular momentum axis of the host's halo (i.e., the reverse of the Holmberg effect).

The outline of the paper is as follows. In §2 we describe the SDSS data, the Millennium Run simulation, and the way in which we define images for the luminous host galaxies in the Millennium Run. In §3 we discuss the selection criteria for finding hosts and satellites, and we highlight some of the properties of the host and satellite galaxies in the Millennium Run. In §4 we compute the locations of the satellite galaxies and we compare the results obtained with SDSS galaxies to those obtained with the Millennium Run galaxies. We summarize our results and compare them to previous, similar studies in §5, and we present our conclusions in §6. Throughout we adopt cosmological parameters $H_0 = 73$ km sec^{-1} Mpc^{-1}, $\Omega_{m0} = 0.25$, and $\Omega_{\Lambda 0} = 0.75$.

2. Observational and Theoretical Data Sets

Our goal in this paper is to compute the locations of the satellites of relatively isolated host galaxies for: (i) observed galaxies in our Universe and (ii) theoretical galaxies in a ΛCDM universe. Below we outline the details of the observational and theoretical data sets that are used in our analysis.

2.1. Observed Galaxies: SDSS

The SDSS is a large imaging and spectroscopic survey that has mapped roughly one quarter of the sky. The spectroscopic portion of the SDSS is complete to a reddening–corrected Petrosian magnitude of $r = 17.77$ (see, e.g., Strauss et al. 2002). Our primary observational data set consists of the seventh data release of the SDSS (DR7; Abazajian et al. 2009), including all of the photometric and spectroscopic information for objects with high quality redshifts (zconf > 0.9) that have galaxy–type spectra (specClass $= 2$), $r \leq 17.77$, and redshifts in the range $0.01 \leq z \leq 0.15$.

We use the de–reddened Petrosian *ugriz* magnitudes (e.g., petroMag_r-extinction_r), and we select the position angles, semi–minor axes, and semi–major axes of our galaxies from the Petrosian r–band data. In addition, the IDL code by Blanton et al. (2003; v4_1_4) was used to K-correct the SDSS galaxy colors to the present epoch (i.e., $z = 0$). Further, in some of the analyzes below we will supplement the data provided directly by the SDSS

with stellar mass estimates and star formation rates. Stellar masses are available for the vast majority of the galaxies in the DR7, but at the moment star formation rates are only available for galaxies in the fourth SDSS data release (DR4; Adelman-McCarthy et al. 2006). Therefore, our galaxy sample will necessarily be restricted when we look at the dependence of satellite location on star formation rate. The stellar masses and star formation rates for the SDSS galaxies are publicly available at `http://www.mpa-garching.mpg.de/SDSS/`. Stellar masses in these catalogs were computed using the philosophy of Kauffmann et al. (2003) and Salim et al. (2007). Star formation rates were computed using various emission lines in the SDSS spectra as described in Brinchmann et al. (2004). Throughout our analysis we use the specific star formation rate (SSFR) of the SDSS galaxies, which is defined to be the ratio of the star formation rate (in $M_\odot$ yr^{-1}) to the stellar mass (in solar units), and we use the average values of the likelihood distributions of the total SSFR obtained by Brinchmann et al. (2004).

2.2. Theoretical Galaxies: Millennium Run Simulation

The Millennium Run simulation[1] (MRS) follows the growth of cosmic structure in a ΛCDM "concordance" cosmology ($H_0 = 73$ km sec^{-1} Mpc^{-1},$\Omega_{m0} + \Omega_{b0} = 0.25$, $\Omega_{b0} = 0.04$, $\Omega_{\Lambda 0} = 0.75$, $n = 1$, $\sigma_8 = 0.9$). The simulation was completed by the Virgo Consortium in summer 2004 using the Max Planck Society's supercomputer center in Garching, Germany, and is described in Springel et al. (2005). The simulation follows the evolution of the dark matter distribution from $z = 127$ to $z = 0$ using $N = 2160^3 \simeq 10^{10}$ particles of mass $m_p = 8.6 \times 10^8 h^{-1} M_\odot$. The simulation volume is a cubical box with periodic boundary conditions and a comoving side length of $L = 500 h^{-1}$ Mpc. A TreePM method is used to evaluate the gravitational force law, and a softening length of $5h^{-1}$ kpc is used. The simulation thus achieves a truly impressive dynamic range of 10^5 in length. Since one of our goals is to construct an accurate catalog of simulated host galaxies and their satellites, it is important for us to use a high–resolution simulation that follows the fate of satellite galaxies accurately as they orbit within the halo of the central host galaxy. The combination of high spatial and mass resolution therefore makes the MRS ideal for our purposes.

The stored output of the MRS allows semi–analytic models of galaxy formation to be implemented by collecting the detailed assembly histories of all resolved halos and subhalos, then simulating the formation and evolution of galaxies within these structures for a variety of assumptions about the physics that is involved. The data on the halo, subhalo, and galaxy

[1]http://www.mpa-garching.mpg.de/millennium

populations which have been produced by such efforts can be used to address a wide range of questions about galaxy and structure evolution (e.g., Croton et al. 2006). As part of the activities of the German Astrophysical Virtual Observatory, detailed information about the halos, subhalos, and galaxies have been publicly released for two independent models of galaxy formation (Lemson et al. 2006).

In order to compare to the SDSS, we need to analyze the MRS in the same way in which one would analyze a combined imaging and redshift survey of the observed Universe. To do this, we make use of the MRS all–sky mock galaxy redshift catalog[2] that was constructed by Blaizot et al. (2005) using the Mock Map Facility (MoMaF). The MRS mock redshift survey is intended to mimic the SDSS, having a nearly identical redshift distribution and very similar color distributions for the galaxies. The mock redshift survey incorporates the semi–analytic galaxy formation model of De Lucia & Blaizot (2007) for the MRS galaxies. Therefore, galaxy fluxes in all of the SDSS bandpasses, as well as star formation rates, stellar masses, and B–band bulge–to–disk ratios, are available for the MRS galaxies.

In order to make the most direct comparison to the SDSS, we need to include the galaxy images that one would have in a real observational survey. That is, our goal is to determine the locations of satellite galaxies, measured with respect to the major axes of the images of their luminous host galaxies. There are, however, no actual *images* of the simulated galaxies, and we must therefore *define* images for the MRS host galaxies. As an aid to defining the image shapes, the bulge–to–disk ratios from the semi–analytic galaxy formation model may be used to assign rough intrinsic morphologies to the MRS hosts. Following De Lucia et al. (2006) we therefore use the B–band bulge–to–disk ratios to classify MRS host galaxies with $\Delta M(B) < 0.4$ as ellipticals, where $\Delta M(B) = M(B)_{\rm bulge} - M(B)_{\rm total}$. Similarly, we classify MRS host galaxies with $\Delta M(B) \geq 0.4$ as "non–ellipticals". We also note that visual inspection of the images of the SDSS host galaxies has revealed these objects to be "regular" systems (i.e., ellipticals, lenticulars, or spirals). Therefore, it is reasonable to assume that the non–elliptical MRS hosts are disk systems with significant net angular momentum, and we will treat all non–elliptical MRS hosts as though they were disk galaxies below.

Following Heavens et al. (2000) we assume that elliptical MRS host galaxies share the shapes of their dark matter halos. During a collaborative visit to the Max Planck Institute for Astrophysics (MPA), we were fortunate to be granted access to the particle data files that resulted from the MRS. The enormous size of the particle files precludes them from being made publicly-available; thus, at present, it is only possible to work with the files on site at MPA. During the visit to MPA the particles within the virial radii (r_{200}) of the elliptical

[2]http://www.g-vo.org/Millennium/Help?page=databases/mpamocks/blaizot2006_allsky

MRS host galaxies were identified, and these particles were then used to compute equivalent ellipsoids of inertia for the elliptical hosts. A total of 98% of the elliptical MRS hosts contain more than 1000 particles within their virial radii, so the equivalent ellipsoids of inertia are well–determined. The major axes of projections of these equivalent ellipsoids of inertia onto the sky then define the orientations of the major axes of the elliptical MRS host galaxies.

In the case of the non–elliptical MRS hosts, it is natural to assume that the net angular momentum of the disk will be perpendicular to the disk. In addition, recent numerical simulations have indicated that the angular momenta of disk galaxies and their dark matter halos are reasonably well–aligned (e.g., Libeskind et al. 2007). Furthermore, the disk angular momentum vectors show a tendency to be aligned with the minor axis of the surrounding mass with a mean misalignment of $\sim 25^\circ$ (Bailin & Steinmetz 2005). We, therefore, computed the angular momentum vectors of the halos of the non–elliptical MRS hosts using all particles contained within the virial radii. These were then used to place thin disks within the halos, oriented such that the disks are perpendicular to the net angular momenta of the halos. The major axes of the projections of these thin disks onto the sky then define the orientations of the major axes of the non–elliptical MRS hosts. We note that the angular momentum vectors of the host halos are well–determined, and 62% of the hosts contain more than 1000 particles that were used to compute the angular momentum.

3. Host–Satellite Catalogs

Although the MRS contains full 6–dimensional phase space information (i.e., positions and velocities) for all of the galaxies, such is of course not the case for the observed Universe. That is, since there is no direct distance information for the vast majority of the galaxies in the SDSS, we are forced to select host galaxies and their satellites using proximity criteria in redshift space, rather than real space. Again, in order to compare the simulation results as directly as possible to the results from the SDSS, we select host and satellite galaxies in the MRS in the same way that they are selected in the SDSS. Below we discuss our selection criteria and the resulting catalogs.

3.1. Host–Satellite Selection Criteria

Hosts and satellites are selected by requiring the hosts to be relatively isolated. In addition, hosts and satellites must be nearby one another in terms of projected separation on the sky, r_p, and radial velocity difference, $|dv|$. Throughout we use the Sample 1 selection

criteria from Brainerd (2005). Specifically, hosts must be 2.5 times more luminous than any other galaxy that falls within $r_p \leq 700$ kpc and $|dv| \leq 1000$ km sec^{-1}. Satellites must be at least 6.25 times less luminous than their host, and they must be located within $r_p \leq 500$ kpc and $|dv| \leq 500$ kpc. In order to eliminate a small number of systems that pass the above tests but which are, in reality, more likely to be representative of cluster environments instead of relatively isolated host–satellite systems, we impose two further restrictions: (1) the sum total of the luminosities of the satellites of a given host must be less than the luminosity of the host, and (2) the observed total number of satellites of a given host must not exceed 9. Our selection criteria yield relatively isolated hosts and their satellites, and it is worth noting that both the Milky Way and M31 would be rejected as host galaxies under our selection criteria. We also note that, although we have adopted one particular host–satellite selection algorithm, the results are not particularly sensitive to the details of the selection algorithm (see, e.g., Brainerd 2005; Agustsson & Brainerd 2006, hereafter AB06).

We know from the MRS that the hosts will span a wide range of virial masses and, hence, a wide range of virial radii. Therefore, very different parts of the halos are probed by applying a fixed search aperture of 500 kpc for the satellites. The selection technique that we have used is, however, fairly standard in the literature, has the advantage that it is simple to implement, and does not depend on any specific *a priori* assumption that the luminosity of a galaxy is correlated with its mass. There are some indications from previous studies (e.g., Yang06) that the satellite anisotropy may be a function of radius and we will explore this in the following section.

In addition, the simple host–satellite selection criteria that we adopt allow, at least in principle, for "multi–homed" satellites. That is, in principle a given satellite could be paired with more than one host. In practice, we find that this occurs extremely rarely and the results we present below are completely unaffected by the presence of mutli–homed satellites. Also, it is true that the selection criteria allow for the presence of galaxies with luminosities $L_{\rm host}/6.25 \leq L \leq L_{\rm host}/2.5$ nearby to the host, and these galaxies are not used in our analyzes. In practice $\sim 48\%$ of the hosts have "non–selected" satellites nearby to them. Of the hosts that have non–selected satellites, the vast majority (77%) have only one (54%) or two (46%) non–selected satellites. Because of this, we refer to our host galaxies as being merely "relatively" isolated.

3.2. SDSS Host–Satellite Catalog

In addition to selection criteria above, we require that the images of the SDSS galaxies are not associated with obvious aberrations in the imaging (for which we performed a visual

check). We also require that the host galaxies are not located close to a survey edge (i.e., the host must be surrounded by spectroscopic targets from the SDSS, within the area of interest). We limit our study to the redshift range $0.01 \leq z \leq 0.15$, where the lower limit helps ensure that the peculiar velocities do not dominate over the Hubble flow, and the upper limit simply reflects the fact that very few hosts can be found beyond this redshift. After imposing all of our selection criteria, our primary SDSS catalog consists of 4,487 hosts and 7,399 satellites. Note, however, that the size of the SDSS catalog is reduced when, below, we further restrict our analyzes to SDSS galaxies with measured stellar masses and specific star formation rates (see Table 1).

3.3. MRS Host–Satellite Catalog

We select host and satellite galaxies from the mock redshift survey of the MRS using the same redshift space proximity criteria that we used for the SDSS. Because of the shear size of the simulation, this results in a very large sample consisting of 70,882 hosts (of which 30% are classified as elliptical) and 140,712 satellites. In addition we note that the semi-analytic model of De Lucia & Blaizot (2007) distinguishes each MRS galaxy according to three distinct types: type 0, type 1, and type 2. Type 0 galaxies are the central galaxies of their friends-of-friends (FOF) halos. These objects are fed by radiative cooling from the surrounding halo. Type 1 galaxies are the central galaxies of "subhalos", and they have their own self–bound dark matter subhalo. Type 2 galaxies have been stripped of their dark matter and they lack distinct substructure. In our catalog of MRS host–satellite pairs, 94% of the hosts are the central galaxies of their own FOF halo (i.e., they are type 0 objects). This assures us that our prescription for finding host galaxies is working well. In contrast to the MRS hosts, the MRS satellites are primarily type 1 objects (41% of the sample) or type 2 objects (39% of the sample). That is, the vast majority of the MRS satellites that are selected by proximity to the host in redshift space are, indeed, contained within a larger halo. However, 20% of the MRS satellites are central galaxies of their own FOF halo (i.e., they are type 0 objects). These latter objects are examples of "interlopers" – objects which pass the redshift space proximity tests but which are not necessarily nearby to a host galaxy. Without actual distance information for the galaxies, a certain amount of interloper contamination of the satellite population cannot be avoided. However, since the SDSS and MRS host–satellite catalogs were selected in the same way, we expect that the contamination of the SDSS satellite sample by interlopers will be similar to that for the MRS sample. We will investigate the effects of interlopers on the observed locations of satellite galaxies in §4.2 below.

A summary of the basic properties of the hosts and satellites in the SDSS (left panels) and the MRS (right panels) is shown in Fig. 1. From top to bottom, the panels of Fig. 1 show probability distributions for the number of satellites per host (panels a and b), the redshift distributions of the hosts (panels c and d), the distribution of apparent magnitudes for the hosts and satellites (panels e and f), the distribution of absolute magnitudes for the hosts and satellites (panels g and h), and the distribution of stellar masses for the hosts and satellites (panels i and j). Although the distributions are not identical for the SDSS and MRS, they are sufficiently similar that a direct comparison of the locations of the satellites in the SDSS and the MRS should be meaningful.

One of the great luxuries of simulations (as opposed to observations of the real Universe) is that all the information about the simulated galaxies is known. In the remainder of this section we highlight some of the information about the MRS hosts and satellites that, for the most part, is not known for the SDSS hosts and satellites. Fig. 2 shows the relationship between the halo virial mass and the stellar mass for the MRS hosts (left panel), the dependence of the halo virial mass on absolute r–band magnitude for the MRS hosts (middle panel), and the variation of stellar mass with $(g-r)$ for the MRS hosts (right panel). From Fig. 2, then, it is clear that the stellar mass of the MRS hosts correlates well with the virial mass of the halo and, therefore, the absolute magnitude. In addition, it is clear that the reddest MRS host galaxies are also the most massive hosts in the simulation.

Fig. 3 highlights information that is known about the MRS satellites. To construct this figure, we use only those objects which we consider to be genuine satellites in the host–satellite catalog. We make this restriction for Fig. 3 because here we are interested in the properties of the genuine satellites, not the properties of the interlopers. Here we accept as genuine satellites those objects that are located within a physical distance, $r_{3D} \leq 500$ kpc, of a host galaxy. This is a rather non–restrictive definition of a genuine satellite and is based simply upon a match to the search radius (i.e., $r_p \leq 500$ kpc) that is used in our host–satellite selection criteria (see §3.1). In addition we define the redshift at which the satellite first enters its host's halo to be the redshift at which the satellite first becomes a member of the FOF group of particles to which the host belongs. The top panels of Fig. 3 show that the stellar masses of the MRS satellites correlate well with the absolute magnitude (panel a), $(g-r)$ color (panel b), and the redshift at which the satellites first entered the halos of their hosts (panel c). That is, the more massive is a satellite, the more luminous is the satellite, the redder it is at the present day, and the earlier it first entered the halo of its host. This agrees well with the results of Kang07 from their analysis of the redshifts at which satellite galaxies with various masses and colors first entered the halos surrounding central galaxies in group systems. Fig. 3d) shows that there is a strong correlation of the present–day color of a satellite and the redshift at which it first entered its host's halo; the

very reddest satellites entered the halo more than 10 Gyr in the past, and the very bluest satellites entered the halo within the past 1.5 Gyr. Fig. 3f) shows that the projected distance at which a satellite is found at the present day is also a strong function of the redshift at which the satellite first entered the halo; on average, satellites at $r_p < 50$ kpc entered their hosts' halos ~ 3.5 Gyr earlier than satellites at $r_p \sim 400$ kpc. Fig. 3e) shows the ratio of the satellite to host stellar mass as a function of the redshift at which the satellites first entered their hosts' halos. The majority of host–satellite pairs (84%) have mass ratios ≤ 0.15, and in the case of these pairs there is a monotonic trend of mass ratio with $z_{\rm entry}$: the smaller is the mass ratio, the more recently the satellite entered its hosts' halo. In the case of the small percentage of host–satellite pairs with mass ratios > 0.15, the trend is reversed: the larger is the mass ratio, the more recently the satellite entered its hosts' halo.

4. Satellite Galaxy Locations: Analysis and Results

The location of a satellite galaxy with respect to its host is computed by measuring the angle, ϕ, between the major axis of the host and the direction vector on the sky that connects the centroid of the satellite to the centroid of its host. Throughout we will refer to the angle ϕ as the "location" of the satellite. Because we are simply interested in investigating any preferential alignment of the satellite locations with the semi–major axes of the hosts, ϕ is restricted to the range $[0°, 90°]$. By definition, a value of $\phi = 0°$ indicates alignment with the host major axis, while a value of $\phi = 90°$ indicates alignment with the host minor axis.

Fig. 4 shows the probability distribution for the locations of the satellite galaxies in the SDSS (left panels) and the MRS (right panels) that were selected using the redshift space proximity criteria from §3.1. In this figure we have computed ϕ for all satellites and we have made no subdivisions of the data based on host properties, satellite properties, or the projected distances at which the satellites are found. The top panels of Fig. 4 show the differential probability distributions, $P(\phi)$, where the error bars have been computed from 1000 bootstrap resamplings of the data. Also shown in the top panels of Fig. 4 is the mean satellite location, $\langle\phi\rangle$, along with the confidence levels at which the χ^2 test rejects uniform distributions for $P(\phi)$. The bottom panels of Fig. 4 show the cumulative probability distributions for the satellite locations, $P(\phi \leq \phi_{\rm max})$, along with the confidence levels at which the Kolmogorov–Smirnov (KS) test rejects uniform distributions for $P(\phi \leq \phi_{\rm max})$. It is clear from Fig. 4 that the satellites in both the SDSS and the MRS are located preferentially near the major axes of their hosts, and the effect is detected with very high significance. However, the tendency for satellites to be found near the major axes of their hosts is stronger in the MRS than it is in the SDSS. It is likely that this discrepancy is due to the rather

idealized way in which the MRS host galaxies have been placed within their halos, and may point to a modest misalignment between mass and light in the host galaxies (e.g., AB06, Kang07, Bailin et al. 2005).

4.1. Dependence of the Anisotropy on Host & Satellite Properties

In this subsection we explore ways in which the locations of satellite galaxies may depend upon various physical properties of the hosts and satellites. Fig. 5 shows results for the dependence of satellite location on various properties of the hosts. Results for the SDSS satellites are shown in the left panels of Fig. 5 and results for the MRS satellites are shown in the right panels. The top panels of Fig. 5 show the mean satellite location, $\langle\phi\rangle$, as a function of the host's $(g-r)$ color, computed at $z=0$. In the case of the SDSS satellites, $\langle\phi\rangle$ is a strong function of host color, with the satellites of the reddest MRS hosts exhibiting a large degree of anisotropy, while the satellites of the bluest SDSS hosts are consistent with being distributed isotropically around their hosts. In the case of the MRS satellites, the satellites of red hosts are also distributed much more anisotropically than are the satellites of blue hosts. However, there is also a clear anisotropy present in the locations of the satellites of the bluest MRS hosts that is not seen for the satellites of the bluest SDSS hosts.

The middle panels of Fig. 5 show the dependence of $\langle\phi\rangle$ on the specific star formation rate (SSFR) of the host. Here is it clear that in both the SDSS and the MRS, the mean satellite location is a strong function of the SSFR; the lower the SSFR, the more anisotropically distributed are the satellites. The bottom panels of Fig. 5 show the dependence of $\langle\phi\rangle$ on the stellar mass of the host. From these panels, then, the mean locations of the satellites in both the SDSS and the MRS are functions of the stellar mass of the host; the greater is the mass of the host, the more anisotropic are the locations of the satellites. Overall, the dependence of the mean satellite location, $\langle\phi\rangle$, on host color, SSFR, and stellar mass agrees fairly well between the SDSS and MRS satellites. While the precise values of $\langle\phi\rangle$ are not identical in the two samples, a general trend is clear in both cases. The satellites of hosts that are red, massive, and have low SSFR are distributed much more anisotropically than are the satellites of hosts that are blue, low mass, and have high SSFR.

Our results in Fig. 5e and Fig. 5f are somewhat at odds with the results of Yang06 and Kang07 (i.e., we find that the locations of the satellites are a function of the stellar mass of the host). Yang06 found a weak tendency for the anisotropy in the locations of the satellites of primary galaxies in SDSS group systems to increase with the mass of the halos. In particular, Yang06 found that the mean location of the satellites of primaries with halo masses in the range $1.4\times10^{12}\ M_\odot \leq M \leq 1.4\times10^{13}\ M_\odot$ was $\langle\phi\rangle = 43.1^\circ \pm 0.4^\circ$ while the mean location of

the satellites of primaries with halo masses in the range $1.4 \times 10^{14}\ M_{\odot} \leq M \leq 1.4 \times 10^{15}\ M_{\odot}$ was $\langle \phi \rangle = 40.7^{\circ} \pm 0.5^{\circ}$. That is, an increase in the masses of the halos by a factor of ~ 100 resulted in a decrease in $\langle \phi \rangle$ of $2.4^{\circ} \pm 0.6^{\circ}$. We find $\langle \phi \rangle = 44.4^{\circ} \pm 0.6^{\circ}$ for the satellites of relatively isolated SDSS hosts with $M_{\rm stellar} \sim 3 \times 10^{10}\ M_{\odot}$ and $\langle \phi \rangle = 41.3^{\circ} \pm 0.6^{\circ}$ for the satellites of relatively isolated SDSS hosts with $M_{\rm stellar} \sim 3 \times 10^{11}\ M_{\odot}$; i.e., we see a decrease in $\langle \phi \rangle$ of $3.1^{\circ} \pm 0.8^{\circ}$. We do not know the masses of the halos of our SDSS hosts, but from Fig. 3a (i.e., the correlation of $M_{\rm stellar}$ with $M_{\rm virial}$ for the MRS hosts) we expect that this stellar mass range for our SDSS hosts corresponds to a factor of ~ 30 in halo mass. Therefore, we see a similar decrease in the value of $\langle \phi \rangle$ in only ~ 1 order of magnitude in mass for our sample as Yang06 saw in ~ 2 orders of magnitude in mass for their sample. Based on a simple extrapolation of our results for the satellites of relatively isolated SDSS hosts, we might therefore have expected the satellites in the study of Yang06 to show a greater difference (by factor of ~ 3 to 4) in the dependence of their locations on halo mass.

In their simulation, Kang07 found no dependence of the satellite locations on the masses of the halos that surrounded the primaries, and they explain that this is due to the fact that the greater flattening of the higher mass halos is counterbalanced by the satellites of lower mass halos having locations that are somewhat flatter than the mass of the surrounding halo. In an attempt to understand the discrepancy between our results and those of Kang07, we expand upon our result for the dependence of the satellite locations on host mass in Fig. 6, where we investigate the effects of the host image assignment prescription on $\langle \phi \rangle$ for the MRS galaxies. The left panels of Fig. 6 show results for MRS hosts that are classified as elliptical. These are objects for which the luminous galaxy is assumed to share the shape of the surrounding dark matter halo. The right panels of Fig. 6 show results for MRS hosts that are classified as non–elliptical. These are objects for which the luminous galaxy is assumed to be a thin disk, oriented such that the angular momentum of the disk aligns with the net angular momentum of the surrounding halo. The top panels of Fig. 6 show $\langle \phi \rangle$ as a function of host color. From these panels, it is clear that the satellite anisotropy is stronger for the very reddest elliptical MRS hosts than it is for the bluest elliptical MRS hosts, however there is essentially no dependence on host color for the locations of the satellites of non–elliptical MRS hosts. It is also clear that the satellites of the elliptical MRS hosts show a much greater degree of anisotropy in their locations compared to the satellites of non–elliptical MRS hosts. This is due to the fact that strict alignment of mass and light in the numerical galaxies, as was done for the elliptical MRS hosts, maximizes the anisotropy of the satellite locations (see AB06 and Kang07).

The bottom panels of Fig. 6 show the dependence of the satellite locations on the stellar masses of the MRS hosts. From these panels it is clear that, at fixed host mass, the satellites of the elliptical MRS hosts show a greater degree of anisotropy in their locations than do the

satellites of non–elliptical MRS hosts. In addition, *within a given class of MRS host galaxy* there is no clear trend of $\langle\phi\rangle$ with the stellar mass of the host. That is, the trend with host stellar mass that we see in panel f) of Fig. 5 is due to the fact that the lowest mass MRS hosts are non–ellipticals (whose satellites show a relatively small degree of anisotropy in their locations) while the highest mass MRS hosts are ellipticals (whose satellites show a much greater anisotropy in their locations). The fact that, within a particular image assignment prescription for the MRS hosts, we see no dependence of $\langle\phi\rangle$ on host mass probably explains why Kang07 did not see a strong dependence of the satellite anisotropy on the masses of the central galaxies in their simulation. Kang07 did not assign galaxy types to their central galaxies, and they used the same prescription to assign image shapes to all the luminous galaxies in their simulation.

In Fig. 7 we demonstrate the effect on $\langle\phi\rangle$ if we use the same image assignment scheme for all of the MRS hosts. That is, Fig. 7 shows how $\langle\phi\rangle$ is affected if we do not adjust our image assignment scheme according to whether or not the MRS host galaxy is an "elliptical" or a "non–elliptical". Open triangles in Fig. 7 show the dependence of $\langle\phi\rangle$ on host color (left panel), SSFR (middle panel), and stellar mass (right panel) under the assumption that all MRS host galaxies share the shapes of their dark matter halos. That is, the open triangles in this figure show the resulting values of $\langle\phi\rangle$ if we simply apply the "elliptical" image assignment scheme to all MRS hosts. Open circles in Fig. 7 show the result of simply applying the "non–elliptical" image assignment scheme to all MRS hosts. That is, the open circles show the result that occurs if all MRS hosts are assumed to be thin disks, oriented such that the angular momentum of the disk is perfectly aligned with the net angular momentum of the halo. For comparison, solid squares show the results from Fig. 5 for the SDSS hosts and satellites. From Fig. 7, then, if we adopt the same image assignment scheme for all MRS hosts, independent of their bulge–to–disk ratios, we cannot reproduce the observed dependence of $\langle\phi\rangle$ on host color, SSFR, and stellar mass that we find for the SDSS galaxies. If we use a single image assignment scheme for all MRS hosts, $\langle\phi\rangle$ for the MRS satellites generally has a much weaker dependence on host color, SSFR, and stellar mass than we see in the SDSS, and sometimes the dependence of $\langle\phi\rangle$ on host property is actually opposite to what we see in the SDSS. Fig. 7 then argues rather strongly for the need for two distinct image assignment schemes as we have adopted for the elliptical and non–elliptical MRS hosts. It also suggests that luminous elliptical galaxies and luminous spiral galaxies in the observed Universe are oriented within their dark matter halos in rather different ways.

In Figs. 8 through 10 we expand upon our results in Fig. 5 for the dependence of the satellite locations on host color, and we do this by splitting our sample into "red" hosts and "blue" hosts. To define "red" and "blue", we fit the distributions of $(g-r)$ host colors in the top panels of Fig. 5 by the sum of two Gaussians (e.g., Strateva et al. 2001; Weinmann et

al. 2006). We find that the division between the two Gaussians lies at $(g-r) = 0.7$ for the SDSS galaxies and at $(g-r) = 0.75$ for the MRS galaxies. We therefore define SDSS hosts with $(g-r) < 0.7$ to be "blue" and SDSS hosts with $(g-r) \geq 0.7$ to be "red". Similarly, we define MRS hosts with $(g-r) < 0.75$ to be "blue" and MRS hosts with $(g-r) \geq 0.75$ to be "red". Figs. 8 and 9 then show $P(\phi)$ and $P(\phi \leq \phi_{\rm max})$ for satellites of the red and blue hosts, respectively.

It is clear from Figs. 8 and 9 that the satellites of red hosts have a much stronger preference for being located near the major axes of their hosts than do the satellites of blue hosts. This is true for both the SDSS and MRS satellites. In addition, the MRS satellites show a stronger preference for being located near the major axes of their hosts than do the SDSS satellites. The satellites of blue SDSS hosts are consistent with having an isotropic distribution around their hosts, while the satellites of red SDSS hosts have a strong preference for being located near the major axes of their hosts. Such a disparity in the locations of the satellites of red and blue host galaxies was also found by APPZ, Kang07, Yang06, Bailin et al. (2008), and Siverd et al. (2009), with the satellites of blue hosts showing little to no preference for a particular location relative to their hosts.

In the case of APPZ, small number statistics (i.e., a relatively small number of host–satellite pairs in these studies) prevented them from placing a strong constraint on whether or not the locations of the satellites of blue hosts were, in fact, truly different from the locations of the satellites of the red hosts. The cause of this is two–fold. First, the majority of SDSS hosts are red (see Table 1). Second, the blue hosts tend to have fewer satellites than do their red counterparts. This results in a paucity of host-satellite pairs in which the host is blue. Here, however, our sample of SDSS hosts and satellites is sufficiently large that we can make a definitive statement about the locations of the satellites of blue hosts versus the locations of the satellites of red hosts. To do this, we computed a two–sample KS test using the cumulative probability distributions from the bottom left panels of Figs. 8 and 9. The result is that, at the 99.9% confidence level, the KS test rejects the null hypothesis that the locations of the satellites of red SDSS hosts are drawn from the same distribution as the locations of the satellites of blue SDSS hosts. That is, with high significance, the locations of the satellites of red and blue SDSS hosts are truly different.

Fig. 10 illustrates the underlying cause of the "lack" of anisotropy in the locations of the satellites of the blue SDSS hosts. Here we plot the mean satellite location, $\langle\phi\rangle$, as a function of projected distance. The left panels of Fig. 10 show the results for the satellites of red hosts, while the right panels show the results for the satellites of blue hosts. In the case of the satellites of red hosts, $\langle\phi\rangle$ is largely independent of r_p. Hence, when we average the satellite locations over all projected distances, $r_p \leq 500$ kpc (i.e., as in Figs. 5, 8 and

9), the result is that the satellites of red hosts exhibit a strong degree of anisotropy. In the case of the satellites of blue hosts, however, $\langle\phi\rangle$ is a function of r_p. Satellites of blue hosts that are located at small projected distances have a tendency to be found close to the major axes of their hosts, while satellites of blue hosts with larger projected distances exhibit a different degree of anisotropy. In particular, satellites of blue SDSS hosts that have large values of r_p have a tendency to be found close to the *minor* axes of their hosts, and when the locations of all satellites of the blue SDSS hosts are averaged over all projected distances, $r_p \leq 500$ kpc, the result is consistent with an isotropic distribution (i.e., top left panel of Fig. 9). The satellites of blue MRS hosts show a preference for being located close to the major axes of their hosts for projected distances $r_p < 300$ kpc, but at larger projected distances the satellite locations become consistent with a random distribution. Therefore, the net anisotropy of the MRS satellites of blue hosts is substantially reduced when averaged over all values of $r_p \leq 500$ kpc (i.e., top right panel of Fig. 9).

Fig. 11 shows the dependence of the mean satellite location as a function of various properties of the satellites. Panels a) and b) show the dependence of $\langle\phi\rangle$ on $(g-r)$, panels c) and d) show the dependence of $\langle\phi\rangle$ on specific star formation rate, panels e) and f) show the dependence of $\langle\phi\rangle$ on the stellar mass, and panels g) and h) show the dependence of $\langle\phi\rangle$ on the projected distances at which the satellites are found. As in Fig. 5, there is generally good agreement between the results for SDSS satellites (left panels) and MRS satellites (right panels), with the greatest degree of anisotropy being shown by the reddest, most massive, and lowest–SSFR satellites. The locations of the bluest, least massive, and highest–SSFR satellites show little to no anisotropy. This is in part attributable to the fact that these objects are likely to have been accreted in the very recent past (see, e.g., Fig. 3); however, as we will see in the next section this is also partially attributable to the fact that our blue satellite population is heavily contaminated with interlopers whose effect is to strongly suppress the anisotropy.

Finally, we note that the locations of the satellites are weakly–dependent upon the projected distances at which they are found (panels g and h of Fig. 11), with the satellites found at $r_p \sim 450$ kpc showing less anisotropy than satellites found at smaller projected distances. This is, of course, unsurprising since the objects that are found at large r_p are most likely to be either genuine satellites that have been accreted very recently (see, e.g., panel f of Fig. 3) or interlopers. In addition, we note that, contrary to the claims of Bailin et al. (2008) very few of our SDSS satellites are found at projected distances $r_p < 50$ kpc (see the histogram in Fig. 5g). The lack of SDSS satellites at small projected distances is caused primarily by the fact that fiber collisions prevent the simultaneous measurement of the redshifts of two galaxies that are very close to each other on the sky. So, it is only in regions of the sky that were observed multiple times that satellites with small values of

r_p may be found. Also, because we have performed a visual check of each and every host galaxy, we know for certain that the satellites that we do identify at $r_p < 50$ kpc are, indeed, separate from their host. That is, the satellites at these projected distances are not, say, H-II regions or bright blue knots within the host galaxy that have been misidentified as objects that are distinct from the host galaxy.

4.2. Effects of Interlopers and $z_{\rm entry}$

When discussing the satellites, it is important to remember that at least some fraction of the satellites that are found using the selection criteria in §3.1 are not genuine satellites at all. Rather, they are interlopers that are not necessarily nearby to a host galaxy, but they happen to pass all of the proximity and magnitude criteria in order to be included as satellites in the catalog. In the case of the SDSS satellites, we have no way of knowing which of the satellites in our catalog are real and which are interlopers. In the case of the MRS satellites, however, we have full phase–space information and we know the physical distances of each of the satellites in the catalog from their respective hosts. Until now, all of our calculations of the locations of satellite galaxies in the MRS have included both the satellites that are physically close to host galaxies, as well as the interlopers. This was done in order to better compare the MRS to the SDSS via identical procedures for the identification of hosts and satellites. In this section we will examine the effects of the interlopers on the observed anisotropic distribution of the satellites, as well as the effect of the redshift at which the satellites first entered their hosts' halos.

Here we adopt the same rather non–restrictive definition of a genuine satellite as in §3.3 and we accept as genuine satellites those objects that are located within a physical distance $r_{3D} \leq 500$ kpc of a host galaxy. The mean location of all MRS satellites that are found within $r_{3D} \leq 500$ kpc of a host galaxy is $\langle\phi\rangle = 39.12^\circ \pm 0.08^\circ$, while the mean location of the interlopers is $\langle\phi\rangle = 43.6^\circ \pm 0.1^\circ$. Clearly, then, the presence of the interlopers in the full data set reduces the measured anisotropy in the satellite locations compared to what one would measure in the absence of the interlopers. Interestingly, the interlopers are not randomly–distributed around the hosts. Instead, on average the interlopers show a weak preference for being located near the major axes of the hosts. This is due to the fact that relatively few interlopers are located at extremely large distances from the host galaxies. The median distance of the interlopers from the hosts is only 630 kpc, indicating that by and large they are within the local vicinity of the hosts.

Shown in Fig. 12 are the results for the differential probability distribution, $P(\phi)$, for MRS satellites, with and without the contribution of interlopers. The open points in Fig. 12

show $P(\phi)$, computed using all satellites in the MRS catalog, including the interlopers. The filled points show $P(\phi)$, computed using only the satellites in the MRS catalog that are located within a physical distance $r_{3D} \leq 500$ kpc of their host. Included in each of the panels of Fig. 12 is the value of the mean satellite location, with and without the contribution of interlopers, along with the fraction of satellites in the MRS catalog that are interlopers (i.e., objects which have $r_{3D} > 500$ kpc). As above, the net effect of interlopers is to reduce the value of $\langle\phi\rangle$. The top panels of Fig. 12 show $\langle\phi\rangle$ for the satellites of red MRS hosts (left panel) and the satellites of blue MRS hosts (right panel). The fraction of interlopers is nearly identical; interlopers account for 32% of the satellites of red MRS hosts and 35% of the satellites of blue MRS hosts. The presence of the interlopers reduces $\langle\phi\rangle$ by similar amounts for the satellites of both the red and blue MRS hosts.

We note that the presence of interlopers is not the cause of the reduced anisotropy for the satellites of the blue hosts compared to the satellites of the red hosts. That is, the removal of the interlopers from the MRS sample does not result in the locations of the satellites of blue MRS hosts being the same as those of red MRS hosts. Formally, when the interlopers are removed, the mean location of the MRS satellites surrounding blue hosts differs from the mean location of the MRS satellites surrounding red hosts by more than 20σ. This differs from the conclusions of Kang07 who found that removing the interlopers from their sample resulted in the locations of the satellites of blue central galaxies being the same as the locations of the satellites of red central galaxies. However, as with the dependence of satellite anisotropy on host mass, this difference may be simply attributable to the two different prescriptions that we have used to assign images to the luminous MRS host galaxies. That is, on average, the red MRS hosts are ellipticals and the blue MRS hosts are non–ellipticals. From Fig. 6, then, we would automatically expect the satellites of red MRS hosts to show a greater degree of anisotropy in their locations than the satellites of blue MRS hosts because of the strong correlation of the satellite anisotropy with the host image assignment scheme (i.e., our "elliptical" image assignment scheme maximizes the satellite anisotropy).

The bottom panels of Fig. 12 show $\langle\phi\rangle$ for red MRS satellites (left panel) and blue MRS satellites (right panel). Here the interloper fraction is strikingly different; only 19% of the red MRS satellites are interlopers, while 57% of the blue MRS satellites are interlopers. Therefore, the presence of a large number of interlopers in the sample of blue satellites is a major factor in the reduced anisotropy of blue satellites compared to red satellites (e.g., panels a) and b) of Fig. 11).

As noted by Kang07, the redshift at which a genuine satellite first enters the halo of its host is a strong function of the mass of the satellite and the present–day color of the

satellite. From panels c) and d) of Fig. 3, the more massive the satellite and the redder is its present–day $(g-r)$ color, the earlier the satellite made its first entry into the halo of its host (see also Kang07). One would naturally expect that it would take a few crossing times for satellites to have their trajectories affected to the point where the locations of the satellites would provide a good proxy for the distribution of the mass with the host's halo. For a CDM halo with a mass of $\sim 10^{12} M_{\odot}$ and virial radius $\sim 180 h^{-1}$ kpc, the crossing time will be of order $\tau_{\rm cross} \simeq R/v \simeq 1.7$ Gyr for $v \sim 150$ km sec^{-1}. Therefore, unless the infall of satellites is highly non–spherical, we would expect satellites that arrived within their host's halo within the past billion years should show markedly less anisotropy than satellites that arrived within their host's halo in the much more distant past.

Solid squares in the top panel of Fig. 13 show the mean satellite location, $\langle\phi\rangle$, as a function of the redshift at which the genuine MRS satellites first entered their hosts' halos. From this figure, satellites that first entered their host's halo within the past ~ 1.25 Gyr (i.e., $z_{\rm entry} \sim 0.1$) show considerably less anisotropy than do those which first entered their host's halo at earlier times. Referring to the bottom left panel of Fig. 3, the bluest MRS satellites are those which first entered their host's halo at redshifts $z_{\rm entry} \sim 0.1$, while the reddest MRS satellites are those which first entered their host's halo at redshifts $z_{\rm entry} > 2$. Therefore, it is unsurprising that, after the removal of interlopers with $r_{3D} > 500$ kpc, the degree of anisotropy exhibited by the blue MRS satellites (bottom right panel of Fig. 12, $\langle\phi\rangle = 41.9^{\circ} \pm 0.2^{\circ}$) is considerably less than the degree of anisotropy exhibited by the red genuine MRS satellites (bottom left panel of Fig. 12, $\langle\phi\rangle = 38.2^{\circ} \pm 0.1^{\circ}$). Also shown in the top panel of Fig. 13 is the mean satellite location, $\langle\phi\rangle$, as a function of $z_{\rm entry}$ for the genuine satellites of red MRS hosts (open triangles) and the the genuine satellites of blue MRS hosts (open circles). From this figure, then, it is clear that satellites began arriving within the halos of the red MRS hosts much earlier than did the satellites of blue MRS hosts. The bottom panel of Fig. 13 shows the probability of the entry redshift, $P(z_{\rm entry})$, for the type 1 and type 2 MRS satellites. The type 2 satellites are the objects that have been stripped of their dark matter and, as expected, Fig. 13 shows that $z_{\rm entry}$ is, on average, considerably earlier for the type 2 satellites than it is for the type 1 satellites (which still retain their dark matter).

5. Summary and Comparison to Previous Results

Here we summarize the major results of our study and compare them to results of previous, similar investigations. The major results that we have obtained by computing the mean satellite location, $\langle\phi\rangle$, using all satellites (including interlopers) are:

1. $\langle\phi\rangle$ is a function of the host color, specific star formation rate, and stellar mass. Satellites of red, massive hosts with low SSFR show considerably more anisotropy than do satellites of blue, low mass hosts with high SSFR (Fig. 5).

2. In order to reproduce the observed trends for the dependence of $\langle\phi\rangle$ on host color, SSFR, and stellar mass, we require two distinct image assignment prescriptions for the simulated galaxies: ellipticals share the shapes of their dark matter halos and non–ellipticals have their angular momentum vectors aligned with the net angular momentum of the halo. (Fig. 7)

3. $\langle\phi\rangle$ is a function of the satellite color, specific star formation rate, and stellar mass. Red, massive satellites with low SSFR show considerably more anisotropy than do blue, low mass satellites with high SSFR (Fig. 11).

4. Averaged over all satellites at all projected distances, the locations of the satellites of blue SDSS host galaxies are consistent with an isotropic distribution, while the satellites of red SDSS host galaxies have a strong preference for being found near the major axes of their hosts. At the 99.9% confidence level, the two distributions are inconsistent with having been drawn from the same parent distribution (Figs. 8 and 9).

5. Satellites of blue MRS host galaxies are found preferentially close to the major axes of their hosts, however the degree of anisotropy is considerably less than that shown by the satellites of red MRS host galaxies (Figs. 8 and 9).

6. $\langle\phi\rangle$ for the satellites of red host galaxies is approximately independent of r_p, while $\langle\phi\rangle$ for the satellites of blue host galaxies is an increasing function of r_p (Fig. 10).

The major results that we have obtained with regards to interlopers are:

7. The interloper contamination is similar (32% and 35%, respectively) for the satellites of red MRS hosts and blue MRS hosts (Fig. 12, top panels).

8. Interlopers are not the cause of the different amount of anisotropy shown by the locations of the satellites of blue MRS hosts versus the satellites of red MRS hosts. The genuine satellites of red MRS hosts show considerably more anisotropy than do the genuine satellites of blue MRS hosts, and the significance is greater than 20σ (Fig. 12, top panels).

9. Our host–satellite selection criteria result in 57% of the blue satellites in the MRS catalog being interlopers and 19% of the red satellites being interlopers (Fig. 12, bottom panels).

10. At the 16σ level, the red genuine MRS satellites show considerably more anisotropy in their locations than do the blue genuine MRS satellites (Fig. 12, bottom panels). This is due to the fact that the blue satellites have only recently arrived within their hosts' halos, while the red satellites arrived in the far distant past.

As mentioned above, the general trend for the satellites of red hosts to show considerably more anisotropy than those of blue hosts has been observed by others (e.g., APPZ; Yang06; Kang07; Bailin et al. 2008; Siverd et al. 2009), and our results agree well with these previous results. Further, we have demonstrated conclusively that in the case of relatively isolated host–satellite systems, the satellites of blue host galaxies are distributed differently around their hosts than are the satellites of red host galaxies.

Also as mentioned above, although our results for the satellites of SDSS host galaxies show trends that are very similar to our results for the satellites of MRS host galaxies, the satellites of MRS host galaxies exhibit a greater degree of anisotropy in their locations. This is probably attributable to the simple prescriptions that we have used to define the images of the MRS host galaxies, and may indicate that a certain degree of misalignment of the galaxy images from our idealized prescriptions is necessary (see also AB06 and Kang07). To estimate the degree of misalignment that is necessary for the anisotropy of the locations of the satellites of the MRS galaxies to match those of the SDSS galaxies, we add Gaussian–random errors to the orientations of the MRS host galaxy images (as viewed in projection on the sky). When we do this, we find that a mean misalignment of $|\delta\theta| \sim 20^\circ$ (measured relative to the "idealized" MRS host image) reduces the anisotropy in the locations of the satellites of the MRS hosts to the point that, when averaged over $r_p \leq 500$ kpc, the result agrees with the result for the satellites of SDSS hosts. We note that, although we have phrased this in terms of a misalignment of the host galaxy image from the idealized prescription, this should not be strictly interpreted as the mass and light of the SDSS galaxies being misaligned by an average of $\sim 20^\circ$. While there may be some degree of true misalignment, it is always important to keep in mind that there are observational errors associated with the measurement of the position angles of observed galaxies, and these can be particularly large in the case of very round galaxies, or galaxies with well–resolved spiral arms. Such errors in the determination of the position angles of the SDSS galaxies will, therefore, contribute some amount to a need for misalignment of the host images in the MRS in order to match the observations. Unfortunately, errors for the position angles of the SDSS galaxies are not yet available in the data base, so we are unable to estimate the contribution of position angle

errors to the value of $|\delta\theta|$ above.

Although our work is very similar in spirit to that of Kang07, we arrive at some different conclusions. First, we find that the degree of anisotropy in the satellite locations depends upon the stellar mass of the host galaxy, while Kang07 found no dependence of the satellite locations on the mass of the surrounding halo. The discrepancy between our theoretical results and the theoretical results of Kang07 is probably due to the fact that we have chosen to use two different image assignment schemes for the MRS hosts (ellipticals vs. non–ellipticals), while Kang07 use the same image assignment scheme for all of their central galaxies. We find that *within a given image assignment scheme* there is no dependence of $\langle\phi\rangle$ on host mass; however, there is considerably more anisotropy shown by the satellites of elliptical MRS hosts than non–elliptical MRS hosts. This, combined with the fact that the least massive MRS hosts are non–ellipticals and the most massive MRS hosts are ellipticals leads to the trend of satellite anisotropy with host mass that we see in the simulation.

In their study of the locations of satellites in SDSS group systems, Yang06 found a rather weak dependence of satellite location on the mass of the surrounding halo; over two orders of magnitude in halo mass, the value of $\langle\phi\rangle$ decreased by only $2.4^\circ \pm 0.6^\circ$. By contrast, we appear to find a somewhat stronger trend of satellite location with host mass. Over ~ 1 order of magnitude in host mass we find a decrease in the value of $\langle\phi\rangle$ that is similar to the value found by Yang06: $3.1^\circ \pm 0.8^\circ$. A simple extrapolation of our results to much higher masses would suggest that over the mass range of their sample, Yang06 should have found a greater change in $\langle\phi\rangle$. The resolution of this discrepancy is unclear, but it could have to do with the fact that we are investigating somewhat different systems (i.e., relatively isolated hosts vs. group environments, where perhaps the central galaxy is not located precisely at the dynamical center). In addition, we use stellar masses to define the masses of our host galaxies while Yang06 derive masses for the halos of their groups using a conditional luminosity function. This discrepancy certainly warrants further investigation in the future, particularly since ΛCDM predicts that the flattening of the dark matter halos of galaxies should increase with halo virial mass (e.g., Warren et al. 1992; Jing & Suto 2002; Bailin & Steinmetz 2005; Kasun & Evrard 2005; Allgood et al. 2006).

Additionally, in their simulation Kang07 find that the reason the satellites of blue central galaxies show less anisotropy than the satellites of red central galaxies is that the presence of a large number of interlopers around the blue central galaxies suppresses the anisotropy. This is because Kang07 find that there is a considerably larger number of interlopers in the sample of satellites around blue central galaxies ($\sim 35\%$) than there are in the sample of satellites around red central galaxies ($\sim 15\%$). When Kang07 remove the interlopers, they find that the degree of anisotropy shown by the genuine satellites of red and blue centrals is

identical. In our work we find a nearly identical interloper fraction for the satellites of red and blue host galaxies (32% for red hosts and 35% for blue hosts). However, it is important to note that we have used a simple non–iterative technique to identify host and satellite galaxies, while Kang07 use a sophisticated, iterative technique which is supposed to reduce the number of interlopers on average. So, it is unsurprising that our relative number of interlopers would differ.

When we remove the interlopers from the MRS host and satellite catalog, we find that the satellites of blue hosts still show much less anisotropy than do the satellites of red hosts. In our analysis, there appear to be two causes of the differences between the locations of the satellites of red and blue hosts. First, $\langle\phi\rangle$ is largely independent of r_p for the satellites of red hosts. Therefore, when $\langle\phi\rangle$ is averaged over all projected distances, $r_p \leq 500$ kpc, the satellites of the red hosts show a great deal of anisotropy. In contrast, $\langle\phi\rangle$ for the satellites of blue hosts is a function of r_p, with satellites located at small r_p being found near the major axes of their hosts and satellites located at larger distances having different locations (nearly isotropic in the case of the MRS satellites, and near the minor axes of the hosts in the case of the SDSS satellites). Therefore, when $\langle\phi\rangle$ is averaged over all projected distances, $r_p \leq 500$ kpc, the satellites of blue hosts show a markedly reduced anisotropy. In addition, we know that the blue MRS hosts are by and large disk systems ("non–ellipticals") and the satellites of the non–elliptical MRS hosts are distributed much less anisotropically than are the satellites of the elliptical MRS hosts due to our image assignment schemes. Thus, as with the discrepancy regarding the trend of satellite anisotropy with host mass, the discrepancy between our results and those of Kang07 for the origin of the different amount of anisotropy shown by satellites of red and blue hosts may be due in large part to the two different assignment schemes that we have used to define the images of the MRS host galaxies.

Now, it is, of course, extremely important not to put too much significance on one data point, especially in the case of a figure in which the data points are inherently correlated. Nevertheless, the value of $\langle\phi\rangle$ for the satellites of blue SDSS hosts that are located at $r_p \sim 400$ kpc is intriguing because it suggests a "reversal" of the anisotropy signal at large distances (right panel of Fig. 10). In their sample of extremely isolated SDSS host galaxies (much more isolated than our sample), Bailin et al. (2008) found no statistically–significant dependence of $\langle\phi\rangle$ on r_p; however, their sample size is much smaller than we have used here (337 hosts and 388 satellites). A weak tendency for the satellites of isolated disk galaxies to be aligned with the minor axes of the hosts was seen by Zaritsky et al. (1997) when the satellite locations were averaged out to large projected distances ($r_p \sim 500$ kpc). More recently, Siverd et al. (2009) found a weak tendency for extremely faint satellites of highly–inclined blue SDSS galaxies to have a minor axis preference when the locations of the satellites were averaged out to similarly large projected distances. This is tantalizing in light of the results of Zhang

et al. (2009) who found that the spin axes of dark matter halos with mass $\lesssim 10^{13} M_{\odot}$ tend to be aligned along the filament in which the halo resides. In addition, Bailin et al. (2008) found that satellites that are most likely to have been accreted recently have a tendency to be found along the same axis as the large–scale structure that surrounds the host galaxy. Thus, a "reversal" of the anisotropy for the locations of the satellites of disk host galaxies at large projected distances could indicate preferential infall of satellites along filaments. Establishing the existence of such a reversal of the anisotropy at large projected distance will, of course, take a great deal more effort (see, e.g., Siverd et al. 2009 who conclude that the discrepancies between previous investigations are largely attributable to sample selection).

We have shown that satellites that are very blue, have low masses and high SSFR tend to show little to no anisotropy in their locations while satellites that are very red, have high masses and low SSFR show a great deal of anisotropy in their locations. Similar results have been seen Yang06, Kang07, and Siverd et al. (2009). Using their simulation, Kang07 interpret this effect to be due to the fact that the reddest, most massive satellites are those which entered their hosts' halos in the far distant past, while the bluest, least massive satellites have only recently arrived within the halo. Our work with the MRS hosts and satellites directly supports this conclusion, however there is an additional component to the effect in our case. The redshift space selection criteria that we have adopted result in the majority of blue satellites (57%) being interlopers, the presence of which reduces the anisotropy exhibited by the genuine blue satellites by a substantial amount (a 7σ effect; see the bottom right panel of Fig. 12).

It is, of course, a tremendous simplification to use the global dark matter halo properties to obtain properties of the luminous central galaxy as we have done here. This is due to the fact that the scale size of the luminous galaxy is far smaller than that of the halo in which it resides. Therefore, it is not necessarily the case that the net halo shape or net halo momentum will be reflected in the shape or angular momentum of the central galaxy. Given these caveats, it is really quite remarkable that such naive prescriptions as we have adopted here give rise to a fair agreement between theory and observation. If nothing else, our results lend credence to the idea that large luminous galaxies have some knowledge of the halo in which they reside, despite the fact that the luminous galaxy may be an order of magnitude smaller in extent than its dark matter halo. While mass may not directly trace light within galaxies, it would not be possible to have such similar results for the locations of satellite galaxies in the observed Universe and ΛCDM if mass and light were not strongly coupled within the host galaxies.

6. Conclusions

Here we have shown that the locations of the satellites of relatively isolated host galaxies in the SDSS and the Millennium Run simulation (MRS) show very similar trends, provided that we adopt two distinct image assignment prescriptions for the MRS hosts: elliptical hosts share the shapes of their dark matter halos while non–elliptical hosts have their angular momentum vectors aligned with the net angular momentum of their halos. If we use only a single image assignment prescription for all MRS hosts, it is not possible to reproduce the dependencies of the mean satellite location on host properties that we see in the SDSS. Averaged over all projected distances, r_p, the degree to which satellites are found preferentially close to the major axes of their hosts is a function of the host's stellar mass, SSFR, and $(g-r)$ color. The satellites of red, massive hosts with low SSFR show a strong tendency for being located near the major axes of their hosts, while the satellites of blue, low–mass hosts with high SSFR show little to no anisotropy in their locations. Red, massive satellites with low SSFR show a strong tendency for being located near the major axes of their hosts, while blue, low–mass satellites with high SSFR show little to no anisotropy in their locations. This last trend can be understood in part by the different times at which satellites entered their hosts' halos. That is, redder, more massive satellites entered their hosts' halos in the far distant past while bluer, less massive satellites have only recently entered their hosts' halos. Therefore, the blue satellites have had their kinematics affected less by their hosts than have the red satellites. In the case of the blue satellites, however, there is an additional factor that reduces the observed anisotropy. From our analysis of the MRS, we expect that the majority of the blue satellites are interlopers, not genuine satellites, and the presence of these objects greatly suppress the value of the measured anisotropy in comparison to the intrinsic anisotropy.

Overall, the presence of interlopers in the satellite catalogs suppresses the degree to which the satellites exhibit an anisotropy in their locations. However, even after the removal of the interlopers from the catalog of MRS satellites, the satellites of blue MRS host galaxies show substantially less anisotropy in their locations than do the satellites of red MRS host galaxies. There are two causes for the reduction of the anisotropy for the satellites of blue hosts versus the satellites of red hosts. First, there is a marked difference of the dependence of the mean satellite location on projected distance for the satellites of red hosts compared to the satellites of blue hosts. In the case of the red SDSS and MRS hosts, the locations of the satellites are largely independent of the projected distances at which they are found. In the case of the satellites of blue SDSS hosts, we find that at large projected distances ($r_p \sim 400$ kpc), there is a tendency for the satellites to be found close to the *minor* axes of their hosts, while at smaller projected distances ($r_p \sim 100$ kpc) the satellites have a tendency to be found close to the major axes of their hosts. The satellites of the blue MRS hosts that

are found at small projected distances are located preferentially close to the major axes of the hosts, while at large projected distances the locations of the satellites are essentially isotropic. Therefore, when the locations of the satellites of blue host galaxies are averaged over all projected distances ($r_p \leq 500$ kpc) there is a substantial reduction in the signal compared to when the locations of the satellites of red host galaxies are averaged over all projected distances.

In addition, we find that the prescriptions we use to assign images to the MRS host galaxies give rise to different degrees of anisotropy in the satellite locations. The satellites of elliptical MRS hosts are distributed much more anisotropically than are the satellites of non–elliptical MRS hosts. Further, the red MRS hosts are by and large ellipticals, while the blue MRS hosts are by and large non–ellipticals. Therefore, at fixed host mass, we find a substantial reduction in the anisotropy of the satellites of blue MRS hosts compared to red MRS hosts due to the different methods by which the luminous host galaxies have been embedded within their halos.

The locations of satellite galaxies with respect to the symmetry axes of their hosts may, at first glance, seem to be a mere curiosity. However, the current investigations are beginning to show that the locations of satellite galaxies can be used as direct probes of the large–scale potentials of dark matter halos, and even provide clues to the orientations of the host galaxies within their halos. Out of necessity, the resulting constraints are statistical in nature (since each host galaxy generally has only 1 or 2 satellites), but this makes the use of satellite galaxies as halo probes very complementary to weak gravitational lensing techniques. Considerably larger samples of hosts and satellites than those used here may reveal a wealth of information about the sizes and shapes of the dark matter halos of the hosts, the orientation of the hosts within their halos, and the history of mass accretion by large, bright galaxies.

Acknowledgments

It is a great pleasure to thank Simon White and the Max Planck Institute for Astrophysics for hospitality and financial support of a collaborative visit that allowed us to work directly with the MRS particle files. We are also very pleased to thank the referee for thoughtful, constructive remarks that truly improved the manuscript. Support under NSF contracts AST-0406844 and AST-0708468 is gratefully acknowledged. Funding for the SDSS has been provided by the Alfred P. Sloan Foundation, the Participating Institutions, NASA, the NSF, the US Department of Energy, the Japanese Monbukagakusho, and the Max Planck Society. The SDSS is managed by the Astrophysical Research Consortium for

the Participating Institutions (the University of Chicago, Fermilab, the Institute for Advanced Study, the Japan Participation Group, The Johns Hopkins University, Los Alamos National Laboratory, the Max Planck Institute for Astronomy, the Max Planck Institute for Astrophysics, New Mexico State University, the University of Pittsburgh, Princeton University, the US Naval Observatory, and the University of Washington. The SDSS Web site is http://www.sdss.org.

REFERENCES

Abazajian, K. Et al. 2009, ApJS, 182, 543

Adelman-McCarthy, J. K. et al. 2006, ApJS, 162, 38

Agustsson, I. & Brainerd, T. G. 2006, ApJ, 650, 500 (AB06)

Allgood, B., Flores, R. A., Primack, J. R., Kravtsov, A. V., Wechsler, R. H., Faltenbacher, A. & Bullock, J. S. 2006, MNRAS, 367, 1781

Azzaro, M., Patiri, S. G., Prada, F., & Zentner, A. R. 2007, MNRAS, 376, L43

Bailin, J., & Steinmetz, M. 2005, ApJ, 627, 647

Bailin, J., Kawata, D., Gibson, B. K., Steinmetz, M., Navarro, J. F., Brook, C. B., Gill, S. P. D., Ibata, R. A., Knebe, A., Lewis, G. F. & Okamoto, T. 2005, ApJ, 627, L17

Bailin, J., Power, C., Norberg, P., Zaritsky, D. & Gibson, B. K. 2008, MNRAS, 390, 1133

Blanton, M. R., Lin H., Lupton, R. H., Maley, F. M., Young, N., Zehavi, I. & Loveday, J. 2003, AJ, 125, 2276

Blaizot, J., Wadadekar, Y., Guiderdoni, B., Colombi, S. T., Bertin, E., Bouchet, F. R., Devriendt, J. E. G., & Hatton, S. 2005, MNRAS, 360, 159

Brainerd, T. G. 2005, 628, L101

Brinchmann J., Charlot S., White S. D. M., Tremonti C., Kauffmann G., Heckman T., Brinkmann J., 2004, MNRAS, 351, 1151

Colless, M., et al. 2001, MNRAS, 328, 1039

Colless, M., et al., 2003, web publication (astro-ph/0306581)

Croton, D. J., Springel, V., White, S. D. M., De Lucia, G., Frenk, C. S., Gao, L., Jenkins, A., Kauffmann, G., Navarro, J. F., & Yoshida, N. 2006, MNRAS, 365, 11

De Lucia, G., & Blaizot, J. 2007 MNRAS, 375, 2

De Lucia, G., Springel, V., White, S. D. M., Croton, D., & Kauffmann, G. 2006, MNRAS, 366, 499

Fukugita, M., Ichikawa, T., Gunn, J. E., Doi, M., Shimasaku, K., & Schneider, D. P. 1996, AJ, 111, 1748

Hawley, D. L. & Peebles, P. J. E. 1975, AJ, 80, 477

Heavens, A., Refregier, A., & Heymans, C. 2000, MNRAS, 319, 649

Hogg, D. W., Finkbeiner, D. P., Schelgel, D. J., & Gunn, J. E. 2001, AJ, 122, 2129

Holmberg, E. 1969 Ark. Astron., 5, 305

Jing, Y. P. & Suto, Y. 2002, ApJ, 574, 538

Kang, X., van den Bosch, F. C., Yang, X., Mao, S., Mo, H. J., Li, C. & Jing, Y. P. 2007, MNRAS, 378, 1531 (Kang07)

Kasun, S. F. & Evrard, A. E. 2005, ApJ, 629, 781

Kauffmann G., Heckman, T. M., White, S. D. M., Charlot, S., Tremonti, C., Peng, E. W., Seibert, M., Brinkmann, J., Nichol, R. C., SubbaRao, M., & York, D. 2003, MNRAS, 341, 33

Lemson, G., & the Virgo Consortium 2006, web publication (astro-ph/0608019)

Libeskind N. I., Cole S., Frenk C. S., Okamoto, T., & Jenkins A., 2007, MNRAS, 374, 16L

MacGillivray, H. T., Dodd, R. J., McNally, B. V. & Corwin, H. G., Jr. 1982, 198, 605

Sales, L. & Lambas, D. G. 2004, MNRAS, 348, 1236

Sales, L. & Lambas, D. G. 2009, MNRAS, 395, 1184

Sales, L., Navarro, J. F., Lambas, D. G., White, S. D. M. & Croton, D. J. 2007, MNRAS, 382, 1901

Salim, S. et al. 2007, ApJS, 173, 267

Sharp, N. A., Lin, D. N. C. & White, S. D. M. 1979, MNRAS, 187, 287

Siverd, R., Ryden, B. & Gaudi, B. S. 2009, astro-ph/0903.2264

Smith, J. A. et al. 2002, AJ, 123, 2121

Springel, V., et al. 2005, Nature, 435, 629

Strateva I., et al., 2001, ApJ, 122, 1861

Strauss, M.A., Weinberg, D.H., et al. 2002, AJ, 124, 1810

Valtonen, M., Teerikorpi, P. & Argue, A. 1978, AJ, 83, 135

Warren, M. S., Quinn, P. J., Salmon, J. K. & Zurek, W. H. 1992, ApJ, 399,405

Weinmann, S. M., van den Bosch, F. C., Yang, X., & Mo, H. J., 2006, MNRAS, 366, 2

Yang, X., van den Bosch, F. C.,Mo, H. J., Mao, S., Kang, X., Weinmann, S. M. & Jing, Y. P. 2006, MNRAS, 369, 1293 (Yang06)

York D. G., et al. 2000, AJ, 120, 1579

Zaritsky, D., Smith, R., Frenk, C. & White, S. D. M., 1997, ApJ, 478, L53

Zhang, Y., Yang, X., Faltenbacher, A., Springel, V., Lin, W. & Wang, H. 2009, ApJ in press (astro-ph/0906.1654)

Table 1: Numbers of Hosts and Satellites

	SDSS		MRS	
	hosts	satellites	hosts	satellites
primary sample (all galaxies)	4,487	7,399	70,882	140,712
galaxies with known $M_{\rm stellar}$	4,412	7,296	70,882	140,712
galaxies with known SSFR	2,421	4,004	47,157	79,812
red galaxies	2,926	2,334	37,022	86,178
blue galaxies	1,561	5,065	33,860	54,534

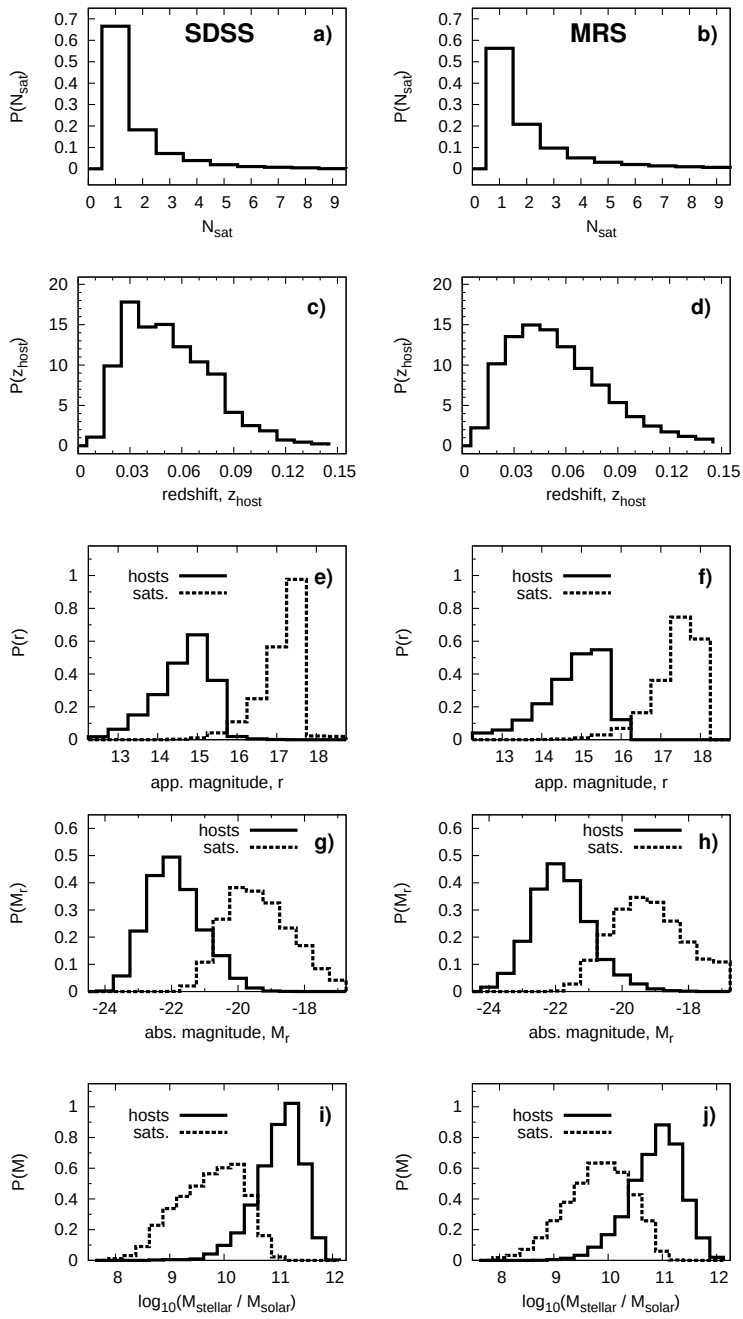

Fig. 1.— Summary of basic properties of the host–satellite pairs in the SDSS (left panels) and the MRS (right panels). From top to bottom, the panels show probability distributions for the number of satellites per host, the redshift distribution of the hosts, the r–band apparent magnitude distributions of the hosts and satellites, the r–band absolute magnitude distributions of the hosts and satellites, and the distribution of stellar masses for the hosts and satellites. In panels e) through j) dotted lines indicate results for the satellites and solid lines indicate results for the hosts.

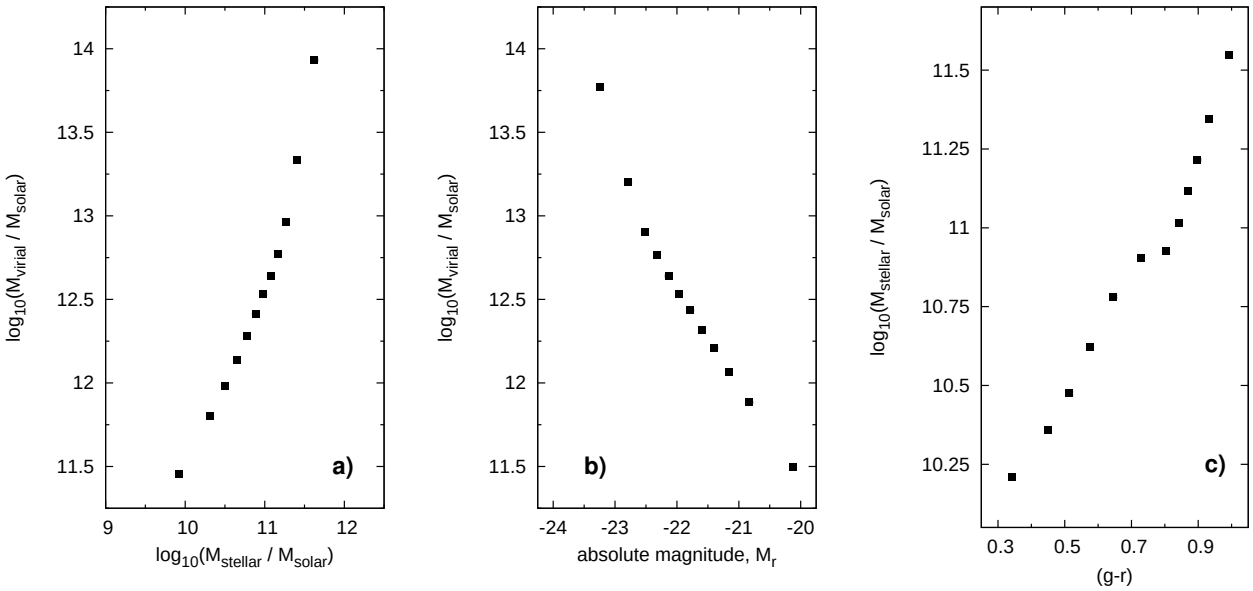

Fig. 2.— Properties of MRS host galaxies. a) Mean host halo virial mass as a function of stellar mass. b) Mean host halo virial mass as a function of absolute r–band magnitude. c) Mean host stellar mass as a function of $(g - r)$, computed at $z = 0$. In all panels the data have been binned such that there are an equal number of objects per bin. In all cases the standard deviations in the mean values are comparable to or smaller than the data points.

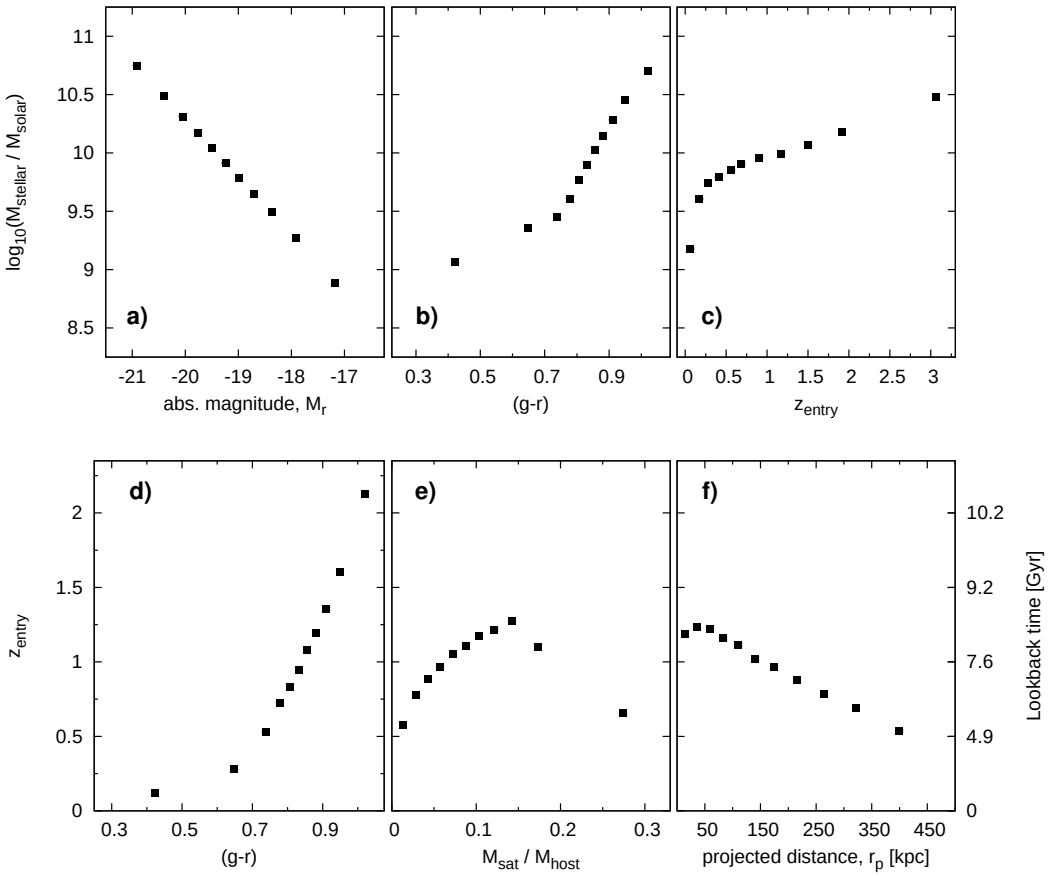

Fig. 3.— Properties of satellite galaxies in the MRS that are located within a physical distance $r_{3D} \leq 500$ kpc of a host galaxy. *Top:* Mean satellite stellar mass as a function of absolute r–band magnitude (panel a), $(g-r)$ at $z=0$ (panel b), and redshift at which the satellite first entered its host's halo (panel c). *Bottom:* Mean redshift at which a satellite first entered the halo of its host as a function of $(g-r)$ at $z=0$ (panel d), ratio of satellite to host stellar mass (panel e), and projected distance at which the satellite is found (panel f). In each panel the data have been binned such that there are an equal number of objects per bin. In all cases the standard deviations in the mean values are comparable to or smaller than the data points.

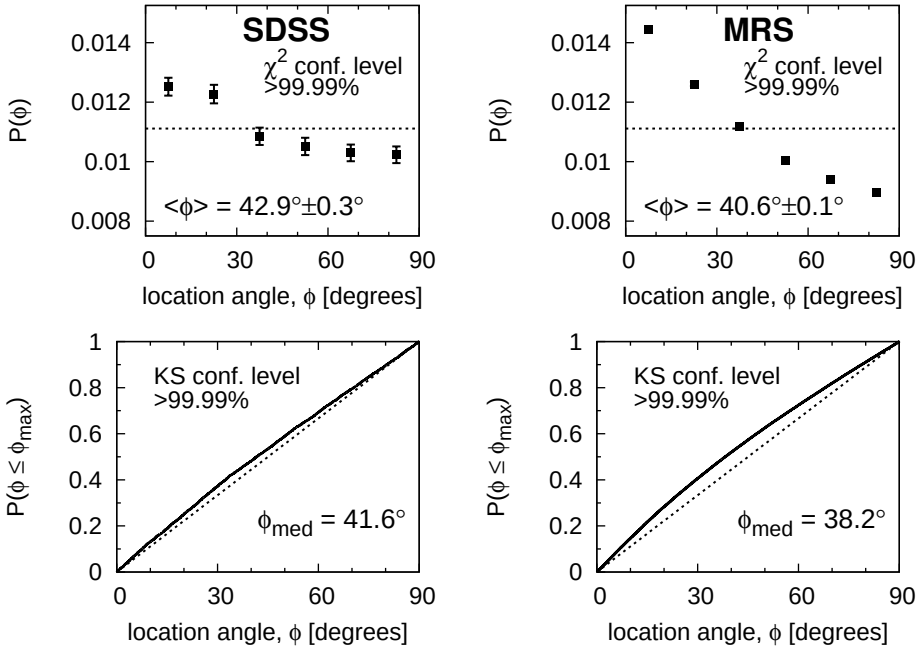

Fig. 4.— *Top:* Differential probability distribution, $P(\phi)$, for the locations of all satellites, measured with respect to the major axes of the hosts. Dotted line shows the expectation for a uniform (i.e., circularly–symmetric) distribution of satellites. The mean satellite location, $\langle\phi\rangle$, and the confidence level at which the χ^2 test rejects a uniform distribution distribution are shown in the panels. Error bars are omitted when they are comparable to or smaller than the data point. *Bottom:* Cumulative probability distribution, $P(\phi \leq \phi_{\rm max})$, for the locations of the satellites with respect to the major axes of the hosts (solid line). Also shown is $P(\phi \leq \phi_{\rm max})$ for a uniform distribution (dotted line). The median satellite location, $\phi_{\rm med}$, and the confidence level at which the KS test rejects a uniform distribution are shown in the panels. *Left:* Satellites in the SDSS. *Right:* Satellites in the MRS. All satellites with $r_p \leq 500$ kpc have been used in the calculations.

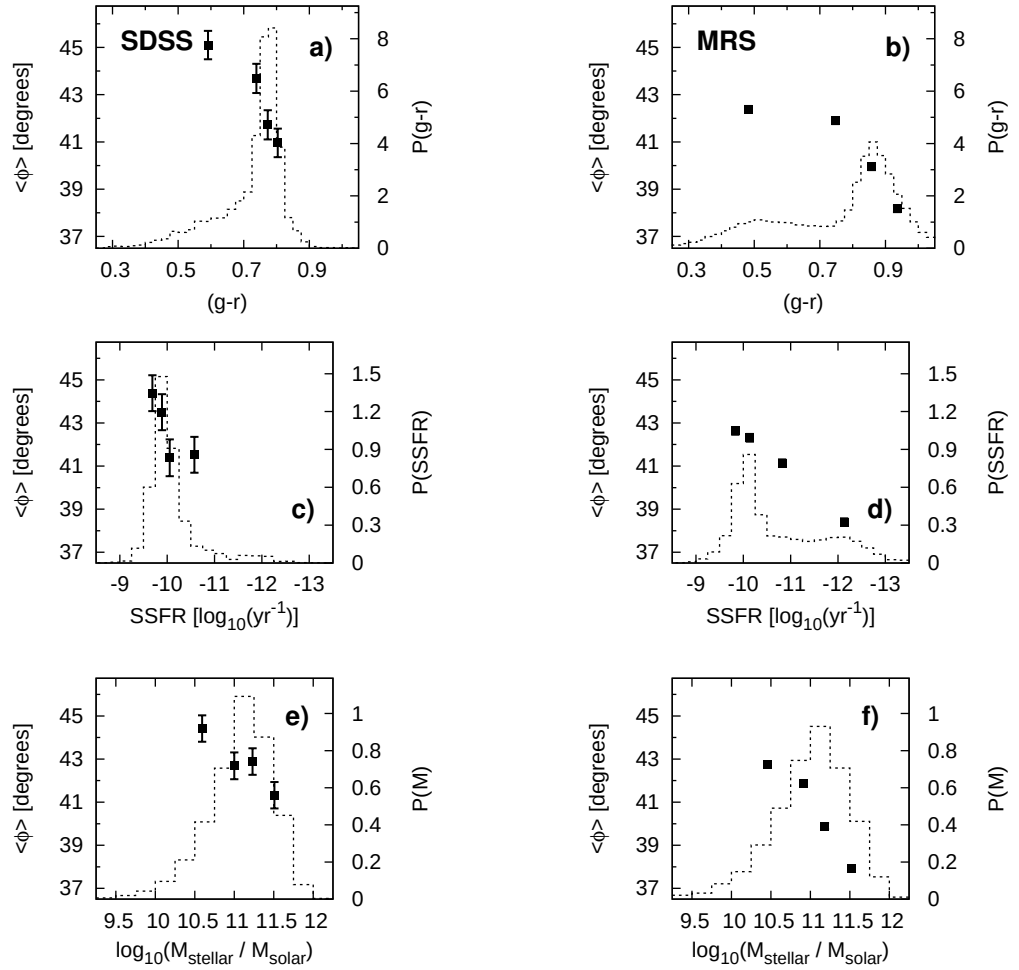

Fig. 5.— Data points with error bars show the mean satellite location, $\langle\phi\rangle$, for SDSS satellites (left panels) and MRS satellites (right panels), as a function of various properties of the hosts. Histograms show the distribution of the host property in each panel. *Top:* $\langle\phi\rangle$ as a function of the host's $(g-r)$ color, computed at $z=0$. *Middle:* $\langle\phi\rangle$ as a function of host specific star formation rate, SSFR. *Bottom:* $\langle\phi\rangle$ as function of host stellar mass. All satellites with $r_p \leq 500$ kpc have been used in the calculations. In each panel the data have been binned such that there are an equal number of objects per bin in the calculation of $\langle\phi\rangle$. Error bars are omitted when the standard deviation in the mean value of ϕ is smaller than the data point.

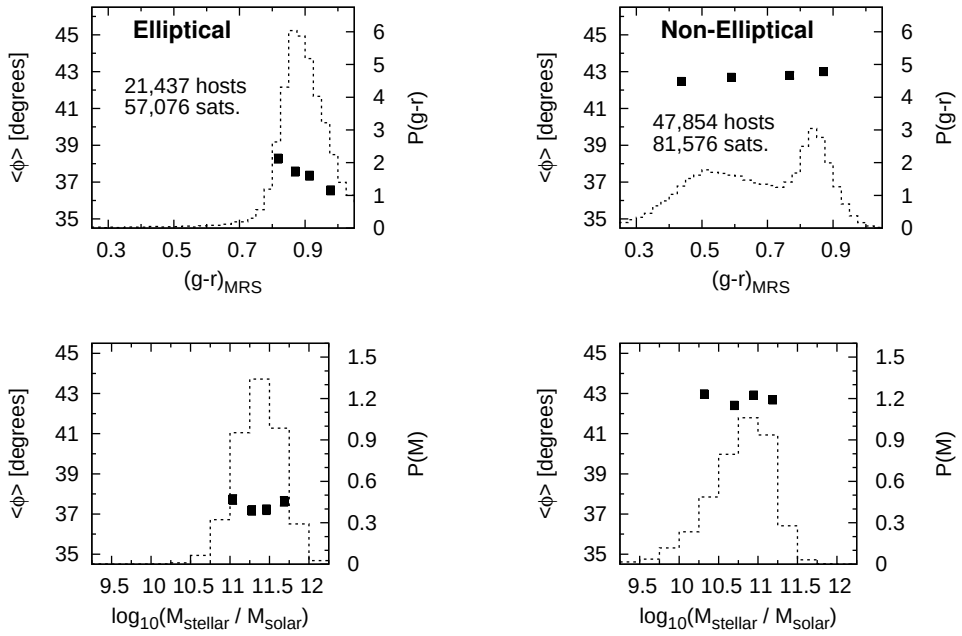

Fig. 6.— Data points show the mean satellite location, $\langle\phi\rangle$, for MRS satellites as a function of host properties for elliptical MRS hosts (left panels) and non–elliptical MRS hosts (right panels). Histograms show the distribution of the host property in each panel. *Top:* Mean satellite location as a function of host $(g-r)$ color. *Bottom:* Mean satellite location as a function of host stellar mass. All satellites with $r_p \leq 500$ kpc have been used in the calculations. In all panels the data have been binned such that there are an equal number of objects per data point. In all cases the standard deviation in the mean value of ϕ is comparable to or smaller than the data points.

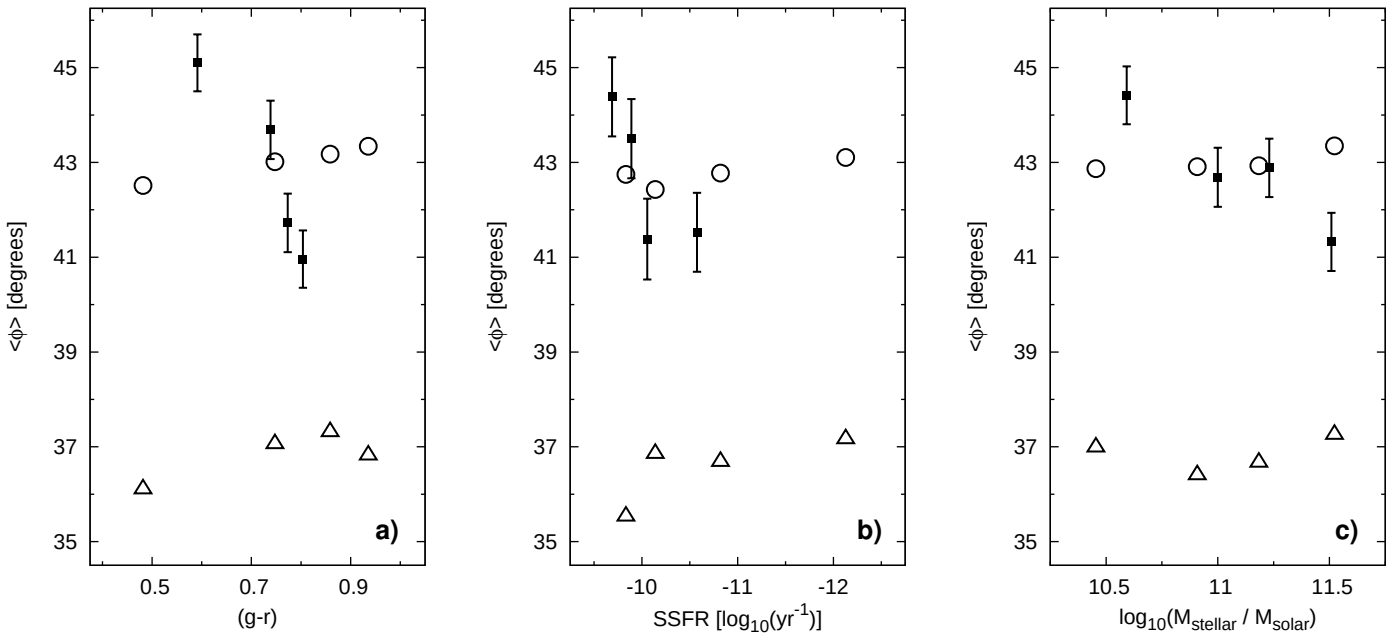

Fig. 7.— Same as Fig. 5, except here single image assignment prescriptions are used to define the major axes of the MRS hosts. Open circles: Major axes of all MRS hosts are obtained from projections of circular disks onto the sky, where the angular momenta of the disks are aligned with the angular momenta of the halos. Open triangles: Major axes of all MRS hosts are obtained from projections of the halo equivalent ellipsoids onto the sky. Solid squares: SDSS results from Fig. 5. Error bars are omitted when the standard deviation in the mean value of ϕ is comparable to or smaller than the data point.

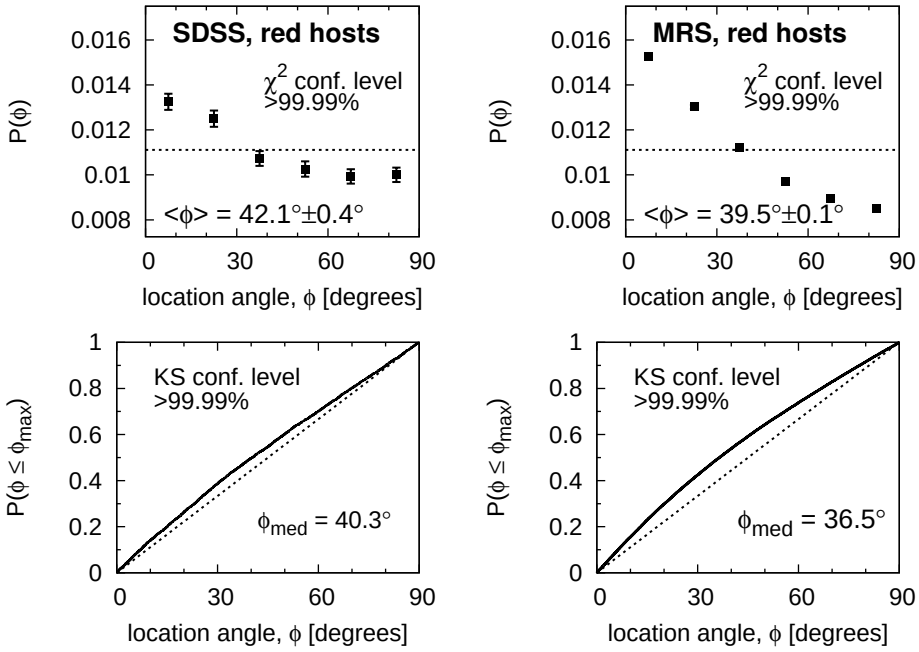

Fig. 8.— Same as Fig. 4, but for the satellites of red hosts. All satellites with projected distances $r_p \leq 500$ kpc have been used in the calculations.

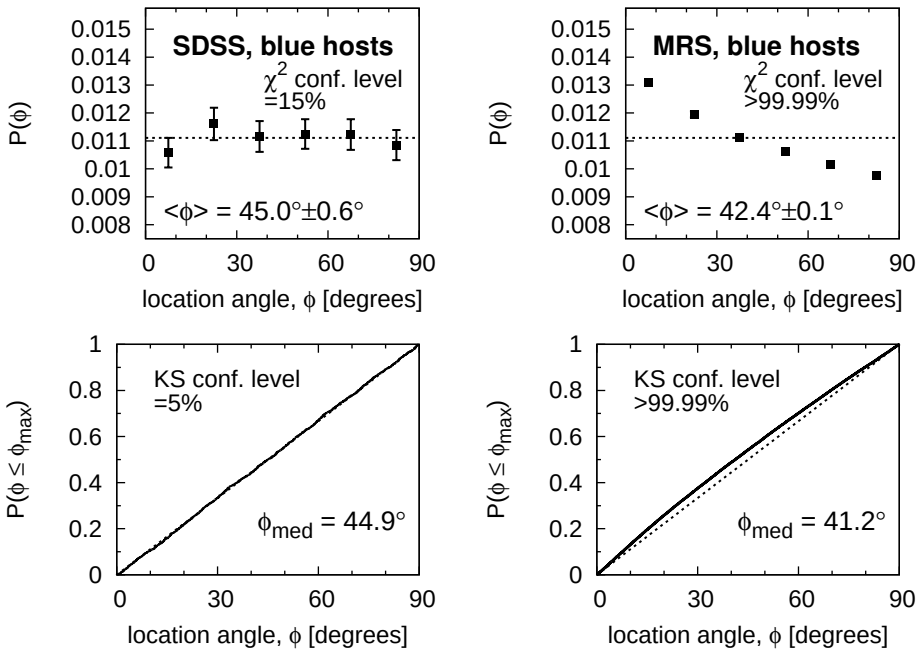

Fig. 9.— Same as Fig. 4, but for the satellites of blue hosts. All satellites with projected distances $r_p \leq 500$ kpc have been used in the calculation.

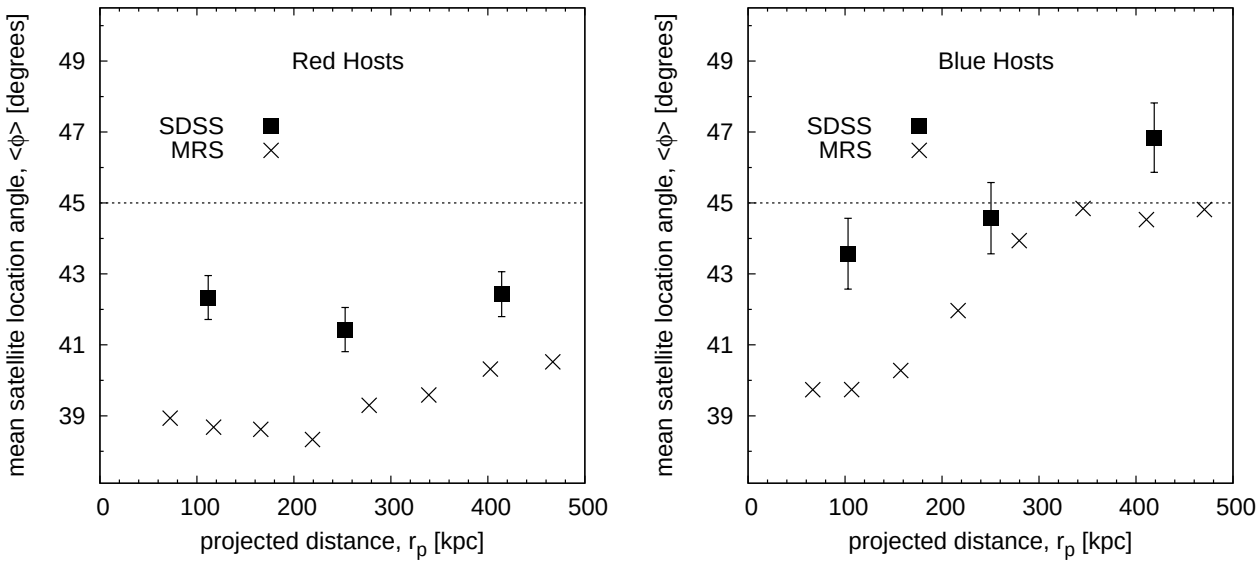

Fig. 10.— Mean satellite location as a function of projected distance, r_p, for the satellites of SDSS hosts (solid squares) and MRS hosts (crosses). *Left:* Satellites of red hosts. *Right:* Satellites of blue hosts. Error bars are omitted when the standard deviation in the mean value of ϕ is comparable to or smaller than the data point.

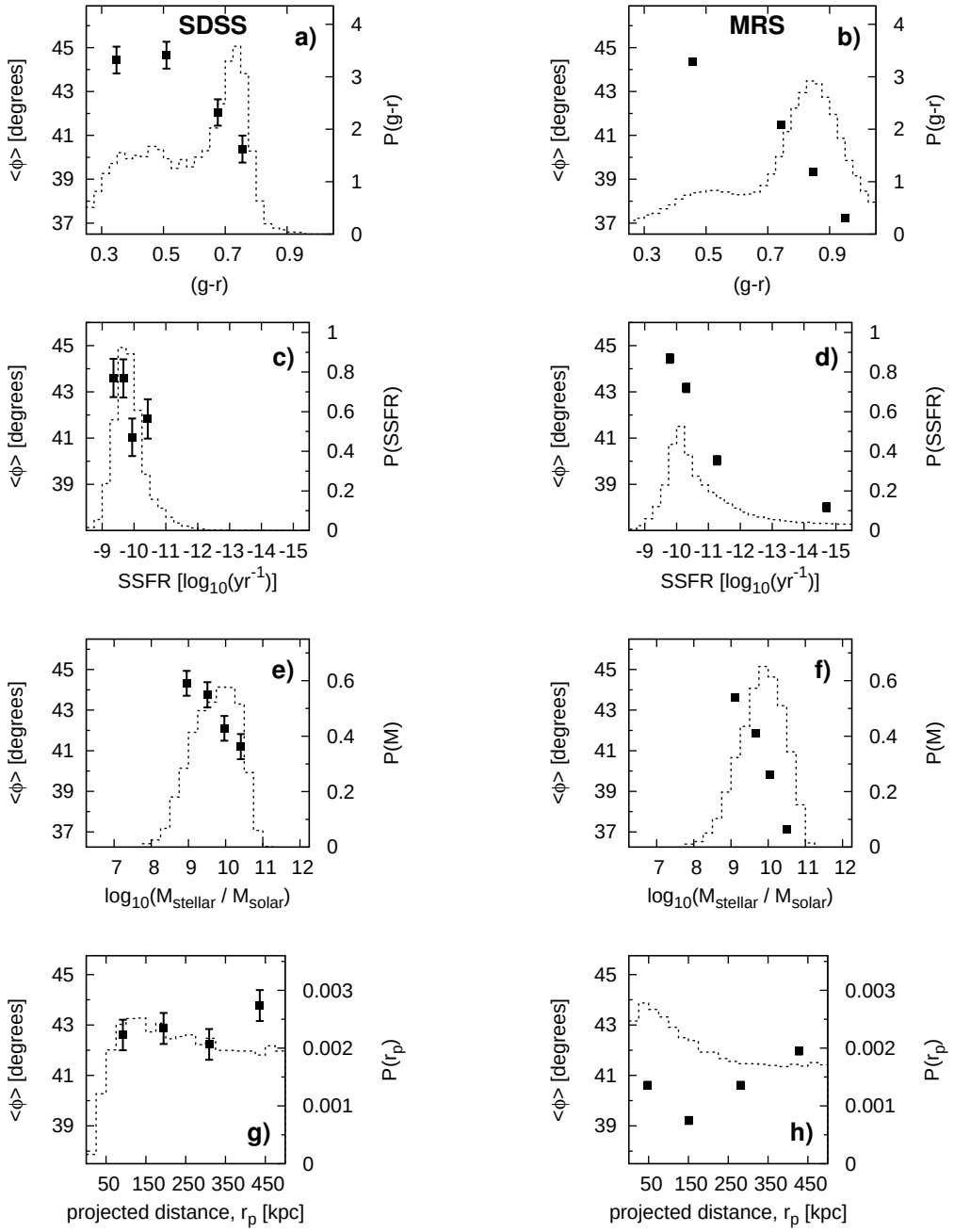

Fig. 11.— Data points with error bars show the mean satellite location, $\langle\phi\rangle$, for SDSS satellites (left panels) and MRS satellites (right panels), as a function of various properties of the satellites. Histograms show the distribution of the satellite property in each panel. From top to bottom the panels show $\langle\phi\rangle$ as a function of $(g-r)$, $\langle\phi\rangle$ as a function of satellite specific star formation rate (SSFR), $\langle\phi\rangle$ as as a function of satellite stellar mass, and $\langle\phi\rangle$ as a function of the projected distance at which the satellites are found. In each panel the data have been binned such that there are an equal number of objects per bin in the calculation of $\langle\phi\rangle$. Error bars are omitted when the standard deviation in the mean value of ϕ is comparable to or smaller than the data point.

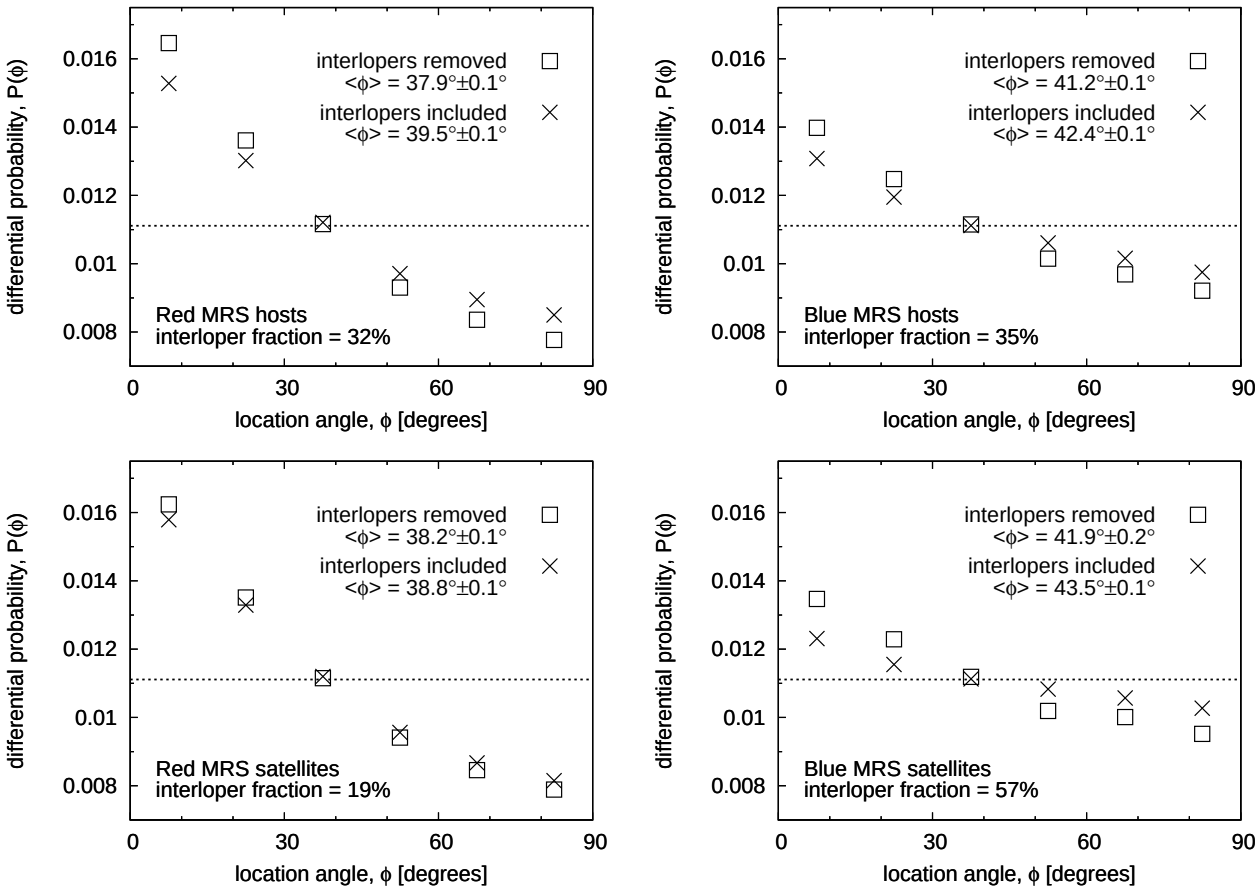

Fig. 12.— Effects of interlopers on the satellite locations in the MRS. Open points show $P(\phi)$ using all objects that were identified as satellites according to the selection criteria in §3.1. In all cases the error in $P(\phi)$ is smaller than the data points. Solid points show $P(\phi)$ after all interlopers have been removed from the satellite sample (see text). *Top panels:* $P(\phi)$ for red (left) and blue (right) MRS hosts. *Bottom panels:* $P(\phi)$ for red (left) and blue(right) MRS satellites.

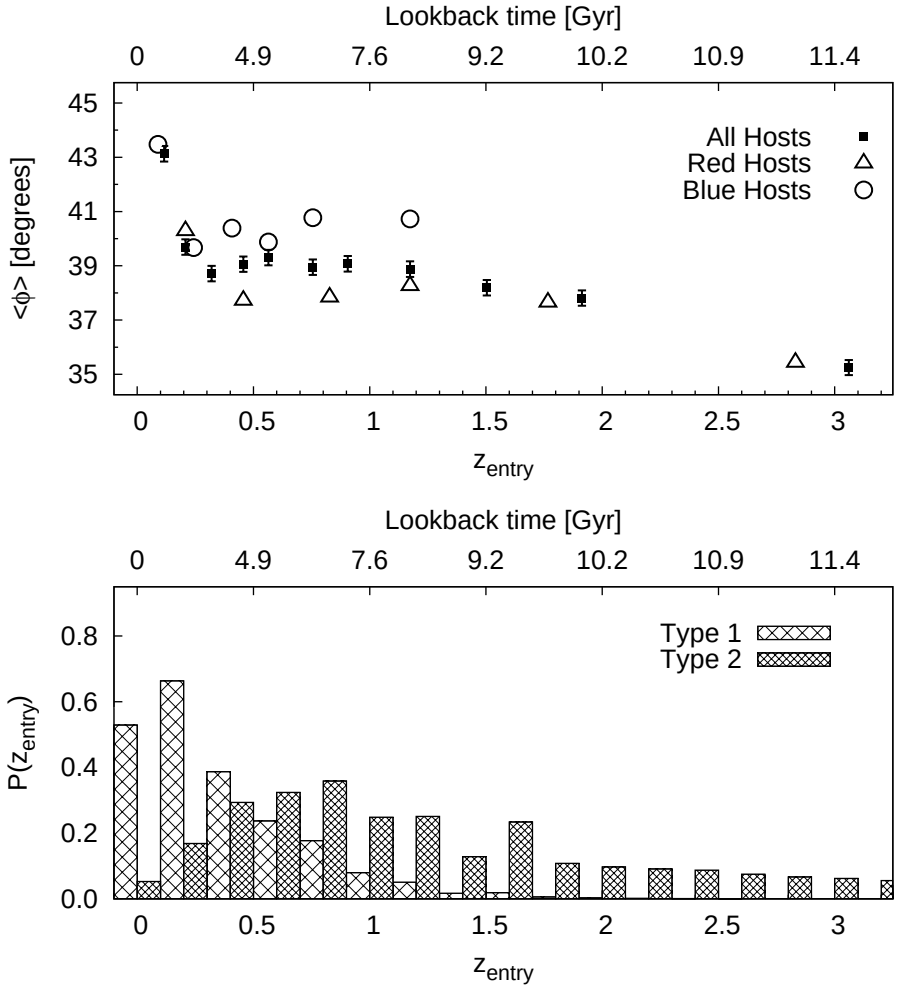

Fig. 13.— *Top:* Mean satellite location at $z = 0$ for genuine MRS satellites as a function of the redshift at which they first entered their host's halo. Here all satellites are located within a physical distance of $r_{3D} \leq 500$ kpc of the host at the present day. The data have been binned such that there are an equal number of objects per bin, and error bars are omitted when the standard deviation in the mean value of ϕ is comparable to or smaller than the data point. Solid squares: satellites of all MRS hosts. Open circles: satellites of blue MRS hosts. Open triangles: satellites of red MRS hosts. *Bottom:* Probability distribution for the redshift at which the genuine MRS satellites first entered their host's halo.